CZECH TECHNICAL UNIVERSITY IN PRAGUE

FACULTY OF ELECTRICAL ENGINEERING

Department of Circuit Theory

Characterization of Photovoltage of Si-V Optical Centers in Diamond Thin Films

Charakterizace fotonapětí Si-V optických center v tenkých vrstvách diamantu

Master's thesis

Study program: Medical Electronics and Bioinformatics
Specialisation: Medical Instrumentation

Master's thesis author: Bc. Maxmilian Marek
Master's thesis supervisor: prof. RNDr. Bohuslav Rezek, Ph.D.

Prague 2023

MASTER'S THESIS ASSIGNMENT

I. Personal and study details

Student's name:	**Marek Maxmilian**
Personal ID number:	**466410**
Faculty / Institute:	**Faculty of Electrical Engineering**
Department / Institute:	**Department of Circuit Theory**
Study program:	**Medical Electronics and Bioinformatics**
Specialisation:	**Medical Instrumentation**

II. Master's thesis details

Master's thesis title in English:

Characterization of Photovoltage of Si-V Optical Centers in Diamond Thin Films

Master's thesis title in Czech:

Charakterizace fotonapětí Si-V optických center v tenkých vrstvách diamantu

Guidelines:

(1) Optical color centers in diamond are functional defects in the crystal lattice that absorb and emit light in an otherwise transparent diamond. They have interesting physical properties with a range of potential applications from quantum communication to biomedicine. The aim of this work is to investigate the generation of photovoltage associated with Si-V centres with a view to future applications in interacting with organic molecules on the surface of thin films. The objectives of the thesis are:
(2) Get familiar with the current knowledge about Si-V optical centers in diamond, their physical properties, methods of creation in thin films during deposition from chemical vapors, and the effect of the surface on their optoelectronic properties. Also learn about methods for measuring microscopic thin film morphology, work function and photovoltage measurements using a Kelvin probe.
(3) Design a suitable experimental setup and conduct an experiment to measure the work function and photovoltage on Si-V centers in nanocrystalline diamond thin films. Perform Kelvin probe measurements on a series of samples with different thicknesses below 100 nm, with different surface modifications (especially hydrogen and oxygen terminated surfaces), and as a function of time and illumination.
(4) Evaluate the work function and photovoltage (including determination of uncertainty) from the measured data in tables and graphs as a function of thickness and surface modification. Discuss the results as a function of the known depth profile of energy bands below the diamond surface and propose a mechanism for the generation of photovoltage due to Si-V centers. Discuss the applicability of Si-V optical centers in diamond thin films in biomedical engineering.

Bibliography / sources:

[1] S. Stehlik et al., ACS Appl. Mater. Interfaces, 2017, 9, 38842. DOI: 10.1021/acsami.7b14436
[2] S. Stehlik et al., Micromachines, 2018, 9, 281. DOI: 10.3390/mi9060281
[3] C. Bradac et al., Nature Commun. 2019, 10, 5625. DOI: 10.1038/s41467-019-13332-w
[4] I. Aharonovic et al., Reports on Progress in Physics, 2011, 74, 076501. DOI: 10.1088/0034-4885/74/7/076501
[5] E. Bourgeois et al., Adv. Optical Mater., 2020, 8, 1902132. DOI: 10.1002/adom.201902132

Name and workplace of master's thesis supervisor:

prof. RNDr. Bohuslav Rezek, Ph.D.   Department of Physics FEE

Name and workplace of second master's thesis supervisor or consultant:

Date of master's thesis assignment:	**20.01.2023**	Deadline for master's thesis submission: **26.05.2023**
Assignment valid until:	**22.09.2024**	

prof. RNDr. Bohuslav Rezek, Ph.D.	doc. Ing. Radoslav Bortel, Ph.D.	prof. Mgr. Petr Páta, Ph.D.
Supervisor's signature	Head of department's signature	Dean's signature

III. Assignment receipt

The student acknowledges that the master's thesis is an individual work. The student must produce his thesis without the assistance of others, with the exception of provided consultations. Within the master's thesis, the author must state the names of consultants and include a list of references.

_____._____
Date of assignment receipt

_____
Student's signature

DECLARATION

I declare that the presented work was developed independently and that I have listed all sources of information used within it in accordance with the methodical instructions for observing the ethical principles in the preparation of university theses.

In Prague on 09.01.2024

....

Maxmilian Marek

ACKNOWLEDGEMENTS

ABSTRACT

SiV (silicon-vacancy) colour centres are optically active defects in the diamond lattice, showcasing unique properties such as high photostability, biocompatibility, and chemical inertness. The potential applications of SiV centres are extensively explored in energy harvesting, biomedicine, and quantum information processing. This thesis investigates the generation of surface photovoltage associated with SiV centres in nanocrystalline diamond layers with different surface chemistry and thickness (6-177 nm). The scanning Kelvin probe proves to be a suitable method for determining surface properties, and is adapted for measuring contact potential difference (CPD) under illumination in a light-dark-light cycle. The initial positive photovoltage undergoes a polarity change at a thickness of around 50 nm, indicating a transition point between surface-controlled and bulk SiV centres. The obtained values are employed to propose a band diagram for photovoltage generation, dependent on the surface chemistry of the samples.

Keywords Kelvin probe, colour centre, nanocrystalline diamond, silicon-vacancy centre, surface photovoltage, work function, hydrogen terminated, oxygen terminated

ABSTRAKT

SiV (křemíková-vakantní) centra jsou opticky aktivní defekty v diamantové matici, které mají unikátní vlastnosti v podobě vysoké fotostability, biokompatibility a také jsou inertní. Použití SiV center je v současné době intenzivně rozvíjené pro širokou oblast použití, od tzv. energy harvestingu, přes biomedicínu až po využití v kvantových informační technologiích. Tato práce zkoumá princip vzniku povrchového fotonapětí způsobeného přítomností SiV center v nanokrystalické dimantové vrstvě s rozdílnou povrchovou úpravou a tloušťkou (6-177 nm). Využita je Kelvin probe metoda, která je vhodná pro analýzu povrchových vlastností materiálů, a je zde implementována pro měření rozdílového kontaktního potenciálu v závislosti na osvětlení v režimu světlo-tma-světlo. Naměřené počáteční pozitivní fotonapětní mění polaritu při tloušťce vzorku kolem 50 nm, která značí zlomový bod mezi povrchovými a hloubkovými SiV centry. Ze získaných hodnot byla vytvořena energetická pásová struktura vzniku fotonapětí v závislosti na tloušťce a povrchové úpravě vzorku.

Klíčová slova Kelvin probe, barevné centrum, nanokrystalický diamant, křemíkové-vakanční centrum, povrchové fotonapětí, work function, vodíková úprava, kyslíková úprava

Contents

List of Abbreviations

Abbreviation	Definition
AFM	Atomic Force Microscopy
CPD	Contact Potential Difference
CVD	Chemical Vapor Deposition
DND	Detonation Nanodiamond
HPHT	High Pressure Hight Temperature
ICP	Inductively Coupled Plasmas
IR	Infra-Red
MCD	Micro Crystalline Diamond
MW	Micro-Wave
NCD	Nanocrystalline Diamond
NEA	Negative Electron Affinity
NV	Nitrogen Vacancy
PEA	Positive Electron Affinity
PL	Photo-Luminiscence
PV	Photovoltage
SCL	Surface Conductive Layer
SEM	Scanning Electron Microscope
SiV	Silicon Vacancy
SPS	Single Photon Source
SPV	Surface Photovoltage
SRIM	Stopping and Range of Ions in Matter
UNCD	Ultra-Nanocrystalline Diamond
UV	Ultra-Violet
VBM	Valence Band Maximum
WD	Working Distance
WF	Work Function
ZPL	Zero-Phonon Line

1. Introduction

Diamond stands out as an interesting material, celebrated for its renowned properties like exceptional hardness and unique optical features. The introduction of lattice defects, known as colour centres, enhances even further its optical characteristics, turning a typically transparent diamond into an optically active material [2]. Among these, the silicon vacancy (SiV) colour centres, formed by placing a silicon atom between two absent carbon atoms in the diamond lattice (vacancies), are extensively researched [3]. These centres exhibit the unique ability to absorb and emit light at specific wavelengths, defining the optical profile of the active centre.

SiV centres present a broad range of applications, ranging from energy harvesting to biomedical uses [1]. The properties of these centres can be adjusted by changing the surface characteristics of the diamond where SiV is incorporated, with modifications such as hydrogenation and oxygenation [1,4]. Various methods are employed to study their properties and the impacts of surface chemistry. A conventional method involves measuring photoluminescence, with its distinct wavelength detectable around ~738 nm. More intriguing methods, include the application of the Kelvin probe method, that offer precise measurements of material surface properties [5].

As photoactive elements, diamond with SiV centres exhibits a surface potential change when illuminated, indicating the generation of photovoltage [1,5]. Limited amount of studies have explored this particular property, including a study performed by Stehlík et al. [5]. The study employed both photoluminescence measurements and the Kelvin probe method to investigate photovoltage in ultra-thin SiV diamond layers (7-40 nm) [1,5]. The results revealed a correlation between the generated photovoltage and both the thickness of the samples and the surface termination.

In this thesis, I further investigate the generation of surface photovoltage associated to SiV centres in nanocrystalline diamond layers with varying surface chemistry and thickness (6-177 nm) [1]. Due to the natural sensitivity of SiV centres to ambient light, I suggested an experiment to measure photovoltage. Utilising a scanning Kelvin probe, I measured the contact potential difference (CPD) during a distinctive light-dark-light cycle [1]. A solar simulator with a wide spectral range of 350-1100 nm was employed to illuminate the samples [1,6].

Work function (WF) and photovoltage (PV) were obtained from the measurements as functions of thickness and surface chemistry. These obtained values were then used to propose a thickness-dependent band diagram model for photovoltage generation with polarity switching [1].

PART I

Theoretical background

2. Diamond

Diamond, an allotrope of carbon, stands out in materials for its fabulous properties, including extreme hardness, high thermal conductivity, and biocompatibility [7,8]. In contrast to expensive natural diamonds, the extensively studied synthetic production methods allow for widespread utilisation. Synthetic diamonds find applications across different fields, from industrial use to state-of-art technologies in science and research.

Carbon as one of the most important elements, being present in materials and processes all around us, is main building block for diamond [7]. Neutral carbon atom has six electrons total, with configuration ($1s^2 2s^2 2p^2$), resulting in four valence electrons [8]. This configuration allows it to create bonds in three different ways (single, double, and triple), and makes it easy to bond also with atoms of other elements [8]. It is also a reason why carbon can create so many different crystalline structures, so called allotropes [7,8].

The three main carbon allotropes are carbine, graphite, and diamond, corresponding to sp, sp^2 and sp^3 hybridisation of atomic orbitals [7,8].

- sp hybridisation: one s-orbital hybridises with one of the p-orbitals to make two sp-hybridised orbitals, the carbon atom bonds by a diagonal symmetry, angle of 180° [7].

- sp^2 hybridisation: trigonal symmetry with one s-orbital is mixed with two p-orbitals to form three hybridised orbitals with angle of 120° [7].

- sp^3 hybridisation: tetrahedral arrangement, forming strongly bonded, entirely covalent face-centred cubic crystal lattice with other tetrahedrals [7].
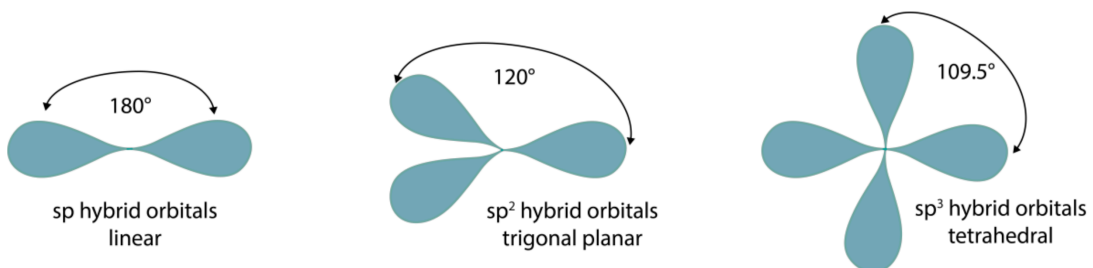

Fig. 1 Visualisation of sp, sp^2, sp^3 hybridisation. Reprinted from [8]

Most of the diamond special properties originate from its rigid structure, but it is not the thermodynamically most stable allotrope of carbon at standard conditions (room temperature and atmospheric pressure) [9]. The most stable form of carbon is graphite, which is by it hybridisation forming sheets that are weakly bonded to each other [9].

The conversion of diamond to graphite results in a reduction in Gibbs free energy, which is more favourable, but because of potential barrier in standard conditions this transformation is negligible [9]. Consequently, diamond stands as the metastable carbon allotrope, posing challenges in its fabrication due to the preference for graphite formation [9].

The primary classification of synthetic diamonds includes the monocrystalline and polycrystalline groups. Monocrystalline diamonds, typically sized around a few millimetres, are created through methods aiming to replicate the physical conditions responsible for natural diamond formation, known as the high pressure high temperature (HPHT) method [7-9]. This process involves applying mechanical pressure on carbon melts generated by heating up graphite [9]. On the other hand, polycrystalline diamonds are usually produced through detonation synthesis, detonation nano diamonds (DNDs), using substances like TNT or RDX [9]. The detonation causes a brief increase in pressure and temperature, facilitating diamond formation from carbon sources introduced during detonation [9]. The resulting diamonds are in the nanometer scale, ranging from 5 to 10 nm [4, 9,10].

Another classification involves the utilisation and production form of synthetic polycrystalline diamonds, categorising them as single particles or as diamond films adhered to a substrate [11]. Regarding diamond films, a further classification based on the size of diamond crystals formed on the surface includes micro crystalline diamond films (MCD), nano crystalline diamond films (NCD), and ultra-nano crystalline diamond films (UNCD) [7-9]. The type of produced film depends significantly on production time and renucleation [7,12]. It's noteworthy that even monocrystalline diamond films can be produced under specific conditions. These films are fabricated using chemical vapour deposition (CVD), a method and principle elaborated in the following chapter. In this thesis, I focus on thin, poly nanocrystalline diamond films (NCDs), seeded on an Si substrate [1,4].

The term also associated with diamond materials is "bulk diamond." It typically refers to monocrystalline diamonds, but it can also be used in the context of diamond layers, where the term is applied to layers with higher thickness or higher volume to surface ratio.
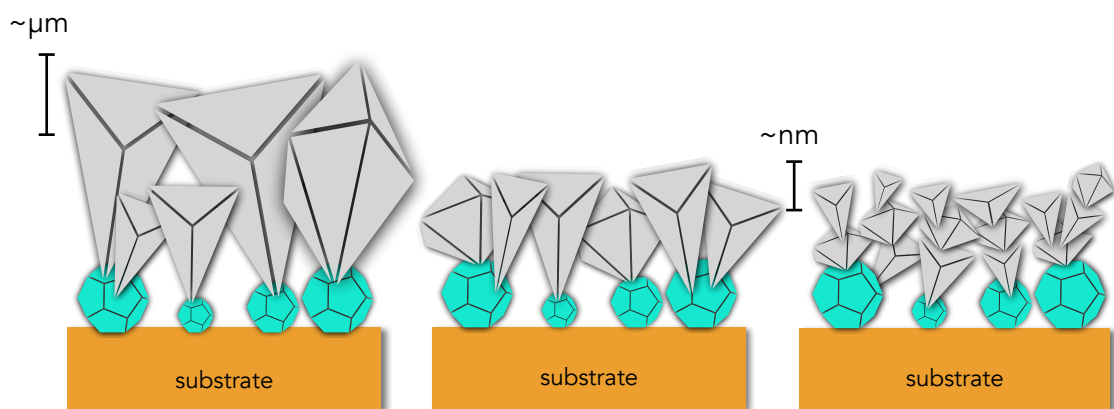

Fig 2 Types of diamond films based on size. From left: MCD, NCD, UNCD. Yellow: substrate, blue: seeded diamonds (DNDs), grey: grown layer. Adapted from [8,13].

While pure diamond acts as an electrical insulator, the use of boron or phosphorus doping transforms it into p-type and n-type conductors, making it a promising material for semiconductor device fabrications [7,9]. With a wide electronic band gap of 5,5 eV, diamond has significant potential for various electronic applications, particularly in optoelectronics [14,15]. Its extreme hardness is used in industrial sector for cutting and drilling tools [9]. Also, diamond's chemical inertness contributes to its biocompatibility, allowing its use in numerous applications in medicine [3]. Not to mention its high thermal conductivity, which makes potential for use as a cooling material in specific applications [7,9]. Diamond also exhibits a relatively high refractive index (n ~ 2.41) in the visible light region, making it well-suited for photonic applications. [7]

2.1. Colour centres in diamond

Diamond has very unique optical properties. Due to its wide band gap of 5.5 eV, it exhibits transparency, allowing the transmission of the entire visible spectrum, along with near-UV and near and short-wavelength IR radiation [3,16]. The band gap also allows for the existence of additional electronic levels in the diamond, resulting in so called crystal lattice defects, known as colour centres [3,17]. The presence of these colour centres alters the crystal's transparency in the visible region, making it show colours. Colour centres are characterised by types of crystal defects, such as impurity atoms (N, Si, Ge, etc.), occupying vacancy locations in the crystal lattice [17]. Vacancies are missing carbon atoms in the diamond's lattice [18].

Optically active colour centres not only absorb light but also have the capability to emit light at specific wavelengths during radiative transitions. Importantly, because the energy of the emitted light lies within the diamond's band gap, the emission from these colour centres is not absorbed.

The energy levels of electronic states within colour centres are precisely defined for individual impurities, leading to the observation of characteristic spectrally narrow zero-phonon lines (ZPL) in the photoluminescence spectra [3]. These ZPLs are usually accompanied by phonon sidebands at longer wavelengths, caused by dissipation of energy during electronic transitions because of lattice vibrations (via phonons) [19-22]. ZPLs are defined in nanometers, corresponding to wavelength of visible light emitted during deexcitation. Colour centres are also characterised by the Debye-Waller factor, indicating the percentage of emission in the ZPL wavelength out of the total emission intensity, including sideband [3,17,22].

Most known colour centre is nitrogen-vacancy colour centre (NV), formed when a nitrogen atom replaces carbon next to vacancy in lattice [3]. It possesses distinctive optical and quantum characteristics and is recognised for its capacity to absorb green light and emit red light [3,9,14]. The NV centre is optically active, offering significant utility in quantum optics applications [3]. It exhibits prolonged electron spin coherence times, making it a promising colour centre for quantum information processing and sensing endeavours [3]. It is also sensitive to magnetic fields, the NV centre holds potential for applications like nanoscale magnetic resonance imaging [3]. On the hand, other centres are known and intensively studied, showing better properties and possible use in another fields where NV is not sufficient.

2.1.1. Group IV centres

Currently, an intensively studied group of colour centres comprises of elements from group IV [17]. Among these, the most analysed and well-known from the group is the silicon-vacancy centre (SiV), marking the first discovery in this category [17]. Later, the germanium-vacancy (GeV) centre, tin-vacancy (SnV) centre, and lead-vacancy (PbV) centre were identified [17]. These colour centres exhibit similar optical properties concerning the zero-phonon line (ZPL) line-width and Debye-Waller factor, while also each having unique characteristics [17].

Defects within group IV diamond configurations adopt the split-vacancy structure, where single element (Si, Ge, Sn, Pb) is located between two adjacent diamond vacancies, corresponding to two missing nearest-neighbour carbon atoms [3,17]. These centres typically possess nominally D_{3d} symmetry, aligning with the diamond <1 1 1> axis as the principal orientation [9,17].

3. SiV centres

The formation of the silicon-vacancy centre occurs when a silicon atom is positioned between two adjacent vacancies within the diamond lattice [3,17]. The most common state is the negatively charged SiV[-] centre, that exhibits a distinctive zero-phonon line (ZPL) at 738 nm, accompanied by a lower phonon sideband centred at 757 nm [3,20]. Also, the Debye-Waller factor at room temperature for this centre is approximately 0,7, representing one of the highest values compared to other recognised colour centres, as noted by Aharonovich [3].

At room temperature, the zero-phonon line (ZPL) exhibits a spectral full width at half maximum around 10 nm, very low value when compared with alternative colour centres [3]. The luminescence wavelength, positioned in the near-infrared spectrum, makes it highly usable for medical applications, given its minimal absorption and background luminescence within tissues in this specific spectral range [3,13,17].
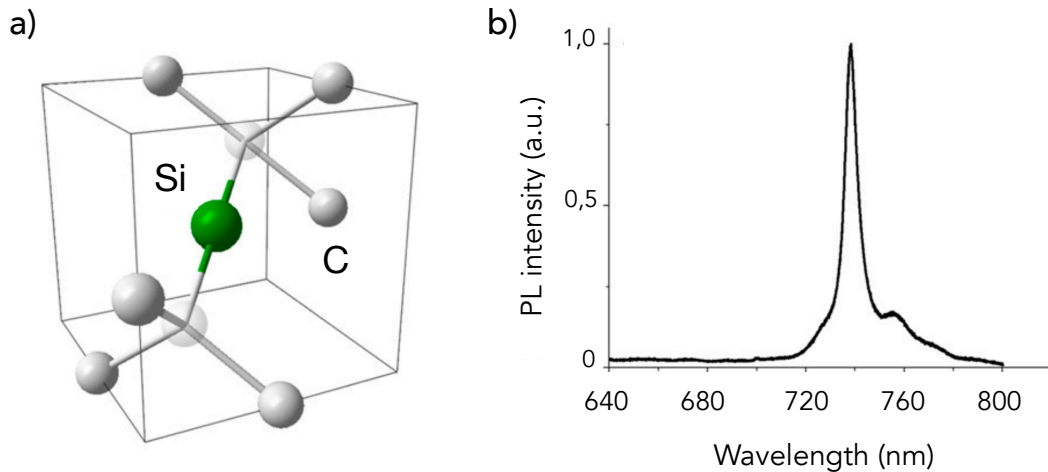

Fig 4 a) SiV centre in diamond lattice formed by silicon in split position between vacancies b) ZPL spectra of SiV centre with peak at 738 nm with side band at 757 nm. Adapted from [3]

Current research suggest that SiV centres are applicable in similar fields as NV centres, functioning as single-photon sources for use in quantum information processing, for sensors and also as biomarkers [3,7,9,13].

Silicon vacancy centres exhibit additional great properties, including excellent spectral stability characterised by nearly lifetime-broadened optical emission [17]. This stability arises from its inversion symmetry (group D_3d), which shields optical transitions from local electric field fluctuations [17]. However, these centres are not without limitations, featuring drawbacks such as low quantum efficiency and abbreviated spin coherence times, typically ranging from 0,5 to 16 ns [1,17,23].

The definitive energy structure of the SiV colour centre is yet to be universally acknowledged, though it can be characterised as an electronic system comprising of three levels, each split by spin-orbital coupling [9,17]. The electron originating from the upper excited state quickly undergoes decay to the photoluminescence (PL) active state [9]. Subsequently, it can either transition radiatively to the ground state or non-radiatively to a shelving state [9]. The presence of a metastable shelving state accounts for the lower photon count rate of SiV centres compared to NV centres [3,9]. This count rate is influenced by the type of diamond hosting the centres, with higher values observed in nanodiamonds, sometimes reaching up to three times more compared to bulk diamond [9,23]. Additionally, SiV centres demonstrate greater stability and emission efficiency in nanodiamonds compared to NV centres [8,13,17].

On the other hand, the work of Trojánek et al. notes that polycrystalline nano-diamond films impact SiV centres due to defects like grain surfaces and sp^2-related defects, common in this diamond type [23]. These defects may act as traps for excited carriers of SiV centres, reducing their internal PL quantum efficiency and increasing film absorption [1,24]. This is significant for thin films with layers of 10-300 nm, for microns, it is negligible [23]. For this reason, monocrystalline diamond is traditionally considered more suitable for optical applications [23].

SiV centres also have a neutrally charged state (SiV^0) with a zero-phonon line (ZPL) at 945 nm [9,17,18]. The fabrication of these centres is challenging and not well-established, and their potential applications remain unclear [9]. Bradac et al. also suggest the possible existence of other silicon-related defects, with ZPLs ranging from 715 nm to 835 nm, also with the divacancy configuration [17].

4. Production of SiV (colour) centres

SiV centres, or colour centres in general, in diamond can commonly be produced by two main approaches: either by incorporating specified impurities during the diamond growth via chemical vapour deposition (CVD) or by implanting targeted ions into the already existing lattice of diamond [9,17].

The aim in the production of colour centres is to precisely control the quantity and location within the diamond. For instance, in quantum computing, there is a demand for single photon emitters, individual colour centres that are easily distinguishable from others [17]. Factors such as ease, scalability of production, and the purity of products also require consideration in fabrication. [17].

4.1.1. CVD

The CVD method is widely used for fabricating pure diamonds, but by incorporating specific atoms during deposition, colour centre rich diamonds can be created. The principle of this process involves forming solid diamond on a solid substrate through deposition from gaseous species [7]. Practically, this occurs by placing a suitably pre-treated substrate into a CVD reactor filled with specific gases, which are then activated into gas species. Activation can be achieved by an external source, such as plasma activation using microwaves or thermal activation using a hot filament [7-9,25]. When optimal environmental conditions, such as the right temperature, pressure, and gas mixture, are met, the produced gas species are transported to the substrate's surface [7,26]. Due to a temperature gradient, gas species react on the surface, forming nucleation centres that grow larger and transform into continuous layers [7,9]. The layer's thickness depends mainly on the deposition time [7].

Gas mixtures present in the process are important for the properties of the produced diamond. The main combination used is hydrogen H_2 with methane CH_4 (concentration usually within 10 %) [8,9]. Methane serves as a source of carbon atoms, while hydrogen enhances the activation of methane and actively etches bonds between carbon atoms, mostly sp^2-hybridised bonds that would otherwise result into growth of the graphite [9]. This mechanism predominantly yields sp^3-hybridised bonds, leading to formation of pure diamond phase [8,9].

When other gases are added into mixture, they can then create colour centres in the diamond, for example SiH_4, N_2, for SiV or NV centres [8]. Other gases can be utilised to incorporate dopants, increasing conductivity or adjusting various properties such as grain size, optical characteristics, and purity by controlling the sp^2-sp^3 phase ratio [8].

The creation of colour centres in diamond during CVD can also be achieved by introducing solid sources of impurities into the chamber [9,26]. For example, clean bare substrates placed inside the chamber or nucleated substrates themselves can serve as a source of Si, as the plasma etches the surface and fills the chamber with Si atoms [1,9].

Because spontaneous nucleation occurs relatively slowly during deposition on a bare substrate, the substrate's surface can be artificially pretreated through a seeding process by covering it with a layer of nano-diamonds [7]. Typically, a mixture of deionised water and diamond powder is applied onto the substrate's surface, often in an ultrasonic bath [1,4]. Diamond nanoparticles created by the DND process, typically around 4-6 nm in size, are commonly used in this seeding process [4,7]. This method enables the rapid creation of diamond films during CVD, as new layers grow directly on the seeded diamonds, resulting in a polycrystalline surface with a random orientation of crystals [7,27]. The layer of seeded diamond is referred to as the nucleation layer. Seeding also facilitates the creation of very thin NCD films, as naturally formed nucleation centres are not evenly distributed on the surface, leading to an uneven and rough surface that hinders continuous growth [4,7,9]. Stehlík et al. demonstrated that controlled annealing in air can reduce former 5 nm DND present in seeding powder to a 2 nm size, opening the possibility for the production of ultra-thin sub-6nm NCD films [4,9].

CVD is a scalable and cost-effective method for creating SiV centres in diamond films with a narrower bandwidth and better optical properties compared to ion transplantation [9]. This is attributed to the incorporation process during growth, which avoids lattice destruction [8]. However, the synthesis of colour centres using the CVD method has one drawback. Due to the main principle of this method, precise positioning of colour centres is not achievable, limiting the potential applications of CVD-made diamond in quantum computing or the field of production of single photon emitters in general [15,17].

Just to note, thicker layers contain more SiV centres, but the concentration of SiV is considered independent of thickness [4].
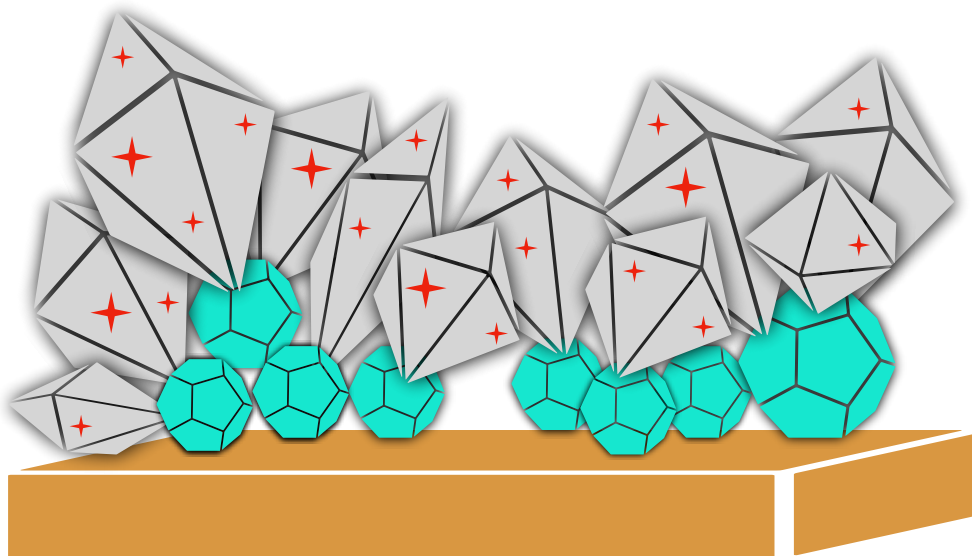

Fig 5. – Visualisation of SiV NCD sample produced by CVD. Yellow: substrate, blue: seeded DND diamonds, grey: deposited nanodiamonds with colour centres, red: SiV centres. Adapted from [1]

4.1.2. Ion implantation

The second method used for colour centre fabrication is the ion implantation. The principle of this method involves bombarding the host diamond with a selected ion accelerated by an electric field targeting it onto the surface and penetrating the diamond [17]. Subsequently, annealing is performed to repair the damage caused by the ion's travel inside the lattice during the bombardment [17]. This annealing process also aims to form colour centres by inducing the movement of vacancies and creating stable, energetically favourable complexes with the implanted ions [9,17].

This method presents an interesting approach for the precise control of the positions of individually implanted single colour centres. The depth of penetration can be accurately determined by calculating the SRIM curve (Stopping and Range of Ions in Matter), which depends on the energy of ions [9,17]. The lateral position is controllable through the ion dose and ion optics [9]. This demonstrates potential for use in quantum applications where single colour centres need to be individually addressed [3]. However, the yield of this method is low, although optical defects reducing colour centres's photoluminescence are lower than compared to CVD [23]. It's worth noting that this ion transplantation method also provides the opportunity to implant colour centres into natural diamonds [13].

4.3. Termination of surfaces

Diamond materials with colour centres created by either of the above-mentioned techniques can be further tuned through a process called termination [28]. This process involves changing surface physicochemical properties such as surface conductivity, work function, and contact angle of the diamond [1,5]. The surface can be terminated with either oxygen or hydrogen.

Hydrogen termination makes the surface positively charged, resulting in negative electron affinity (NEA), and exhibits hydrophobic characteristics with a contact angle of approximately 90° [9,16]. In contrast, oxygen termination creates a negative potential of the surface, positive electron affinity (PEA), and a hydrophilic surface with a contact angle as low as 10° [9,13,29]. The alteration in surface termination is typically achieved through high-temperature annealing, using a hydrogen-rich gas for H-termination or annealing in air for O-termination [7,13,29]. It's worth noting that diamonds produced by CVD are naturally H-terminated. In the context of biomedical applications, oxidised surfaces are more prone to adsorb proteins, cells, DNA, and other bioactive molecules, topics that will be discussed later [3,13].

The surface termination also significantly influences colour centres in diamonds and their activity. Stehlík et al. discovered that the photoluminescence (PL) of nanocrystalline diamond (NCD) layers, estimated to be around 10 nm thick, can be fully activated or deactivated by simply changing the surface termination [5]. Bing Yang et al. also observed that H-terminated surfaces exhibit reduced or zero PL around 738 nm, a wavelength characteristic of the SiV centre's zero-phonon line (ZPL), compared to O-terminated surfaces [30]. This suggests that SiV centres close to the surface (<10 nm) are positioned above the Fermi level, causing excited electrons to be trapped within holes in the surface conductive layer (SCL) [1,5,31,32]. Changing the termination of the diamond to oxygenated results in a significant increase in the PL level for

SiV⁻ centres [5]. This implies that the excited levels of SiV are positioned below the Fermi level, allowing electrons to occupy them and subsequently emit at 738 nm during deexcitation [1,5]. The objective of this research is to further investigate the impact of surface termination on colour centres to gain a better understanding of a principle that is not yet exactly defined.

5. Biomedical Applications

Diamonds, in general, are a promising material for biomedical applications due to their properties, including chemical inertness, biocompatibility, nanometer size, and surface functional groups [33]. These qualities make diamonds well-suited for applications such as biomarking, drug delivery, biosensors, tissue engineering, and more [13,33].

The surface of diamonds can be easily functionalised through termination, leading to a change in surface wettability and affinity [8,34]. Hydrogen-terminated surfaces exhibit hydrophobic behaviour, making them less prone to adsorb water and other proteins common in biological tissues [13]. Conversely, oxygen-terminated surfaces are capable of forming polar interactions with their surroundings, resulting in the adsorption of various biological species, proteins, and chemicals [8,13].

One of the studied applications of diamond is in tissue engineering, where a direct interaction between cells and the diamond surface is wanted [13]. In the work of Penissi et al., a broad application of nanocrystalline diamond films is discussed [13]. When the surface of nanodiamond films is tuned using appropriate chemistries or cell-adhesion ligands, they can be utilised for applications of cell adhesion to a material surface, both in vitro and in vivo [13]. These films were employed with bone-derived cells, resulting in improved proliferations and higher activity growth, making them suitable for use in bone implants, supported also by the hardness and wear resistance of diamonds [13]. The interaction of such surfaces was also explored for soft tissues and neuronal interfaces [13].

Interest in the use of diamonds in medical applications is also attributed to nanoscale size of diamond particles. This small size allows diamond particles to diffuse through the cell membrane and enter living cells [3]. Due to their excellent biocompatibility, these particles remain within the cells and are not trapped by endosomes, as demonstrated in the study by Faklaris et al. [3,35]. The functional groups on the surface create the possibility for a wide variety of chemical compounds to be attached to them, making them suitable for highly efficient drug delivery [3,33,35].

Biomarking is another widely studied application of nanodiamond particles [9]. Current biomarkers used in fluorescence microscopy, like fluorescent proteins or organic dyes, are effective but have a major drawback: lack of long-term photostability [8,16,36]. Nanodiamonds with colour centres offer an ideal solution as they are photostable, transparent, and exhibit low cytotoxicity [13]. Another crucial parameter in biomarking is the spectra of absorbance and emitted light [3]. Biological structures in cells, such as collagens, proteins, and flavins, absorb light in the wavelength range of 300-500 nm and fluorescence in the range of 400-550 nm [3]. Therefore, biomarkers should absorb at more than 500 nm and emit at longer than 600 nm, as indicated by the work of Aharamovich et al. [3]. This condition is met by the NV colour centre, but it is not ideal due to its lower count rate in nanodiamonds and low Debye-Waller factor [3]. Much more suitable is the use of SiV centres, which have a strong zero-phonon line (ZPL) in the near-infrared light spectra [3,33]. This is hardly absorbed by living tissues and differs significantly from tissue autofluorescence [33]. Additionally, SiV centres have higher brightness than NV centres [3,37].

Bradac et al. also mention the possibility of using different colour centres with various functional groups simultaneously in the same cell, and then employing optical filters to select the desired biomarker [17].

The optical transparency of diamonds is also a significant advantage for biomarkers, as it allows the use of optical microscopes without influencing the image [17].

Diamonds find another application in biomedicine as biosensors [8,13]. Their advantages enable the monitoring of cell cultures "in vivo" without negative effects, and the diamond surface can be easily tailored for various applications [8]. Biosensors categories include electrochemical, mechanical, DNA and protein sensors, as well as cell culture sensors [8].

6. Kelvin Probe

The Scanning Kelvin Probe is a state-of-the-art device employed for measuring the surface electrical potential and topography potential of a sample, offering non-contact scanning capabilities [38]. It provides valuable insights into defects, adsorbates, and compositional differences by revealing local variations in work function [38]. These measurements prove highly beneficial in studying dynamic charge-trapping behaviours, surface coating properties, and corrosion effects [5,24,38].

The fundamental principle of the measurement involves the use of a vibrating capacitor [38]. A thin probe with a circular-shaped end is positioned near the sample surface, forming a parallel plate capacitor [38,39]. The potential difference between materials generates charge on the probe tip [38]. As capacitance is inversely dependent on the distance between capacitive layers, applying oscillations to the probe leads to a change in distance, resulting in a change in charge and producing of measurable current [38]. Since the probe is made from a stable metal with an unchanging work potential, the measured current can be used to calculate the surface potential of the sample [38].

The original approach to measuring CPD involves attempting to achieve zero charge between the vibrating tip and the sample by applying a constant potential and adjusting it until no detectable electrical current is present in the circuit [38]. Applied potential is called backing potential [38,39]. However, this method is highly sensitive to external electric fields, which can generate current in the circuit and influence the measured values [38]. Sources of noise include background noise and components of the Kelvin Probe itself [38].

A more modern approach is currently employed, using an "off-null" detection method that measures the generated signal far from the balance point [38,39]. Since the amplitude of the generated current has a linear dependence on the backing potential, the CPD value can be easily determined through simple interpolation [38]. This approach enables higher signal levels with an improved signal-to-noise ratio. Additionally, it facilitates the measurement of the distance between the probe and the sample, important for precise control of the distance and ensuring the reproducibility of measurements by preventing variations due to uneven spacing [38,39].

The Kelvin probe measures the CPD, which is equal to the difference in work function between the tip and the sample [5,38-40]. By employing a standardised sample with a known work function, it becomes possible to calculate the work function of the tip and, even further, the work function of the sample [1,40].

The work function is a crucial parameter for describing materials. It is defined as the "least amount of energy required to remove an electron from the surface of a conducting material, to a point just outside the metal with zero kinetic energy" [7,9]. As an electron travels to the surface of the sample, its energy is affected by the chemical, electrical, optical, and mechanical characteristics of the region [9]. The work function is extensively used to comprehend surface properties, surface states, photoelectric effects, or conduction properties of the sample's surface [38,41,42]. This information can then be utilised to generate band diagrams.

PART II

Materials and Methods

7. Samples

For this thesis, I used thin SiV NCD films with varying thicknesses of the grown layer, created through the CVD method on Si (100) substrates in a square shape of size 10 by 10 mm [1]. The substrates were cleaned and pretreated in an ultrasonic bath containing deionised water with diamond powder (diameter of 5-10 nm, New Metals and Chemicals Corp. Ltd., Kyobashi) originating from DNDs [1, 43]. The substrates underwent a two-time dilution in the bath [1,43].

Following CVD was conducted in a plasma-enhanced reactor activated by a microwave source (MW, 2.45 GHz) using the ellipsoidal resonator with focused plasma [1]. Diamond films were deposited from a hydrogen-rich plasma with methane (3% CH_4 in H_2, H_2 flow 300 sccm[1)]) at approximately 700 °C, under a total gas pressure of 6 kPa and MW power of 3 kW [1]. A bare, clean Si substrate was also present in the chamber, serving alongside the deposited substrates as a source of Si atoms [1].

Six thin NCD layer samples were prepared by controlling the CVD time within the range of 3 to 15 minutes [1]. The thickness of the grown layer, without a nucleation layer, was evaluated within the range of 6-52 nm. The structure of the fabricated SiV NCD layer is illustrated in Fig. 5 and growth is illustrated in Fig. 6. An additional thick sample was added to the set as a reference, with a known total thickness of 200 nm [1].

The surface of the samples was then treated to different terminations, H-terminated and O-terminated, respectively. For each termination, a set of seven samples was prepared. Oxidation was performed by annealing in an oxygen-rich plasma for 4 minutes in an ICP radio frequency (RF, 13.56 MHz) plasma system with the following parameters: RF power 100 W, pressure 60 Pa, O_2 flow rate 25 sccm [1]. Hydrogen termination was performed for 10 minutes in the same MW plasma-enhanced system used during the CVD fabrication of samples, only in gas without CH_4 addition, with otherwise the same conditions [1].
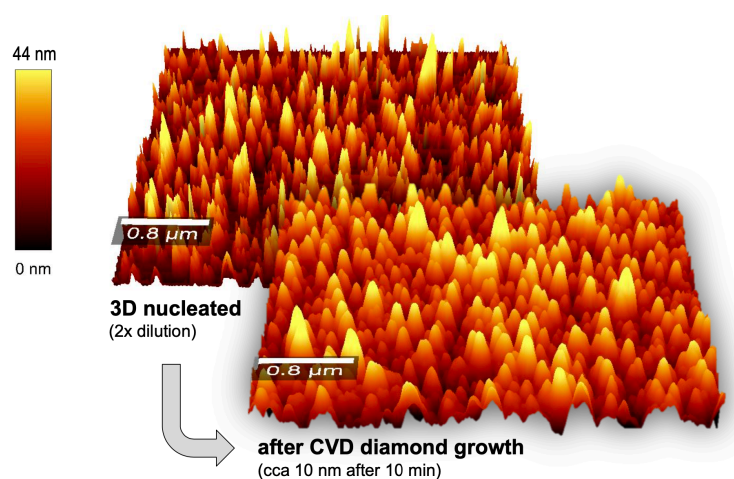

Figure 6. AFM scan of sample after seeding and after CVD growth.
Reprinted from prof. RNDr. Bohuslav Rezek, Ph.D

---

[1] standard cubic centimeter per minute

8. Methods

The objective of this thesis is to evaluate the work function and photovoltage as a function of thickness and surface modulation of SiV NCD layer samples. To achieve this goal, I conducted thickness measurements and Kelvin Probe measurements.

8.1. Thickness Measurements

Scanning electrical microscopy (SEM), a commonly employed method for measuring sub-micro structures, was utilised to obtain the thickness values of the SiV layers in the samples. The measurements were conducted at the Institute of Physics, CAS (Prague, Czech Republic), with assistance from Mgr. Jitka Libertínová.

For thickness measurement, each sample (both modifications) was cut into two pieces using a diamond blade knife, enabling the acquisition of cross-section images [1]. SEM images were captured at a magnification of 200 kX at 10 kV in the regime of secondary electrons with an in-beam detector (Figure 7) [1]. The working distance (WD) was set at 4-5 mm (MAIA 3, Tescan, Czech Republic) [1]. Thickness values were measured at three positions on the sample, with 9 points at each position. Built-in TESCAN software was used for measuring. The values were averaged, and the standard deviation was calculated (values shown in Table 1, a picture of measurement technique is in A.1. Appendices chapter).
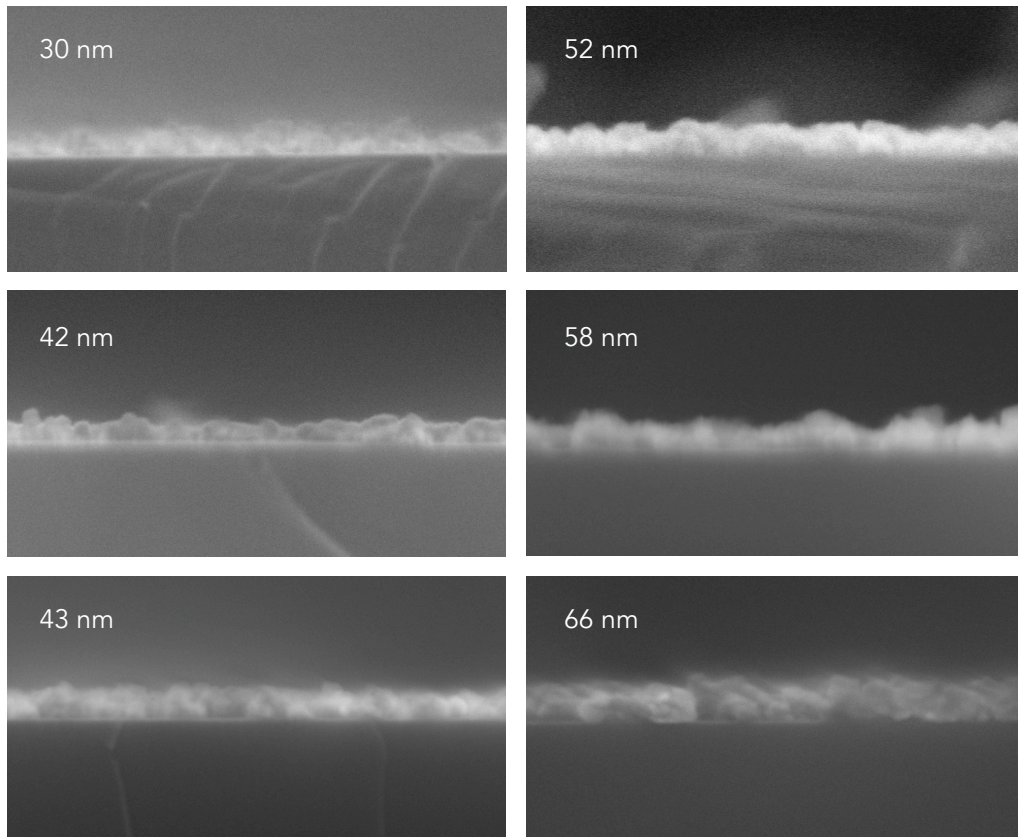

Figure 7. SEM images of cross-section of samples, with average thickness measured.

Obtaining values proved to be quite challenging due to low contrast and the presence of very thin diamond layers [1]. Additionally, determining which height of crystals to select for measurement on the sample was a challenge because the grown layer is not uniform, and the distance of crystals from the cross section plane could not be estimated. As a result, there was a tendency to select larger, highly visible crystals, even from further planes. The difference between terminations also contributed to the difficulty, with hydrogen-terminated samples appearing more blurred, making the edges unrecognisable. Due to these challenges, an alternative method had to be selected.

As a more suitable second method, reflectance interferometry was chosen. The Ocean Optics NanoCalc-XR spectroscopic reflectometer, paired with NanoCalc software, was employed [1]. White light in the 250-1050 nm range with a 90° incidence angle illuminated the thin diamond layer of the sample, allowing the wavelength function of reflected light to be obtained [1,9]. This method provided more representative values, as the measurement covered a larger area compared to SEM [1].

Since both methods measured the entire thickness of the diamond layer film on the substrate, the seeding layer needed to be subtracted to obtain the value for the SiV layer. For this purpose, the previous work by Kromka et al. was referenced, where the thickness of the nucleation layer was studied [12]. The measured nucleation layers ranged from 20 to 30 nm, so, for the purposes of this thesis, the average thickness of the nucleation layer was considered as 25 nm [1,12]. The grown layers of NCD with SiV centres are shown in Table 1.

Table 1. Average measured thickness values of samples.

Sample	1	2	3	4	5	6	7
Total film thickness measured by SEM (nm)	30 ± 2	42 ± 1	52 ± 5	58 ± 8	43 ± 1	66 ± 2	200 ± 5
Total film thickness measured by reflectance interferometry (nm)	31 ± 2	33 ± 2	43 ± 4	54 ± 5	68 ± 5	77 ± 2	202 ± 2
Thickness of grown SiV NCD layer (nm)	6 ± 2	8 ± 1	18 ± 1	29 ± 5	43 ± 8	52 ± 2	177 ± 5

8.2. Kelvin Probe

To obtain work function values for the studied samples, I initially conducted scanning Kelvin Probe measurements under straightforward conditions. Given the sensitivity of SiV centres to light, measurements were carried out in a dark box. Shortly after the initial experiments, a drifting tendency in the measured CPD voltage was observed [1]. Additionally, when the same sample was measured repeatedly at various spots, different values were obtained, as shown in Figure 8.
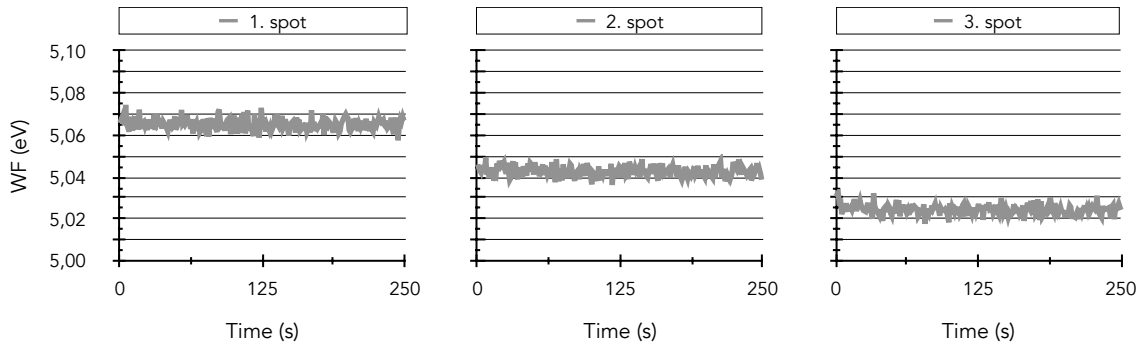
Figure 8. Work function values in three spots on the same sample during one measurement. Decrease is visible, due to high sensitivity of SiV centres to light absorbed during manipulation [44].

The changes and instability observed in the measured work functions were primarily caused by the extreme sensitivity of SiV centres to ambient light in the lab. When the position on the sample was being changed or during the exchange and placement of samples under the probe, the dark box was opened, exposing SiV centres to light. This light exposure led to the absorption of light, causing the accumulation of charge and subsequently changing the surface potential.

To resolve this issue, one potential solution would be to place, store, and manipulate the samples in complete darkness. However, fulfilling such a condition would be highly complicated and impractical. Since one of the objectives of this thesis is to measure the photovoltage of SiV centres, meaning that these centres would need to be exposed to light, I proposed an alternative approach for obtaining work function data. Taking inspiration from the work of Rezek et al., which demonstrated a change in CPD when exposed to a light source, I suggested an "inverse" method [25,45]. Instead of shielding samples from light, they would be fully exposed, leading to a state of supersaturation where most, ideally all, of the SiV centres are in the excited state. The light source would then be turned off, and the response in the form of CPD change would be recorded, allowing for the determination of the photovoltage of the surface SiV centres. The scheme of the suggested experiment is shown in Figure 9.
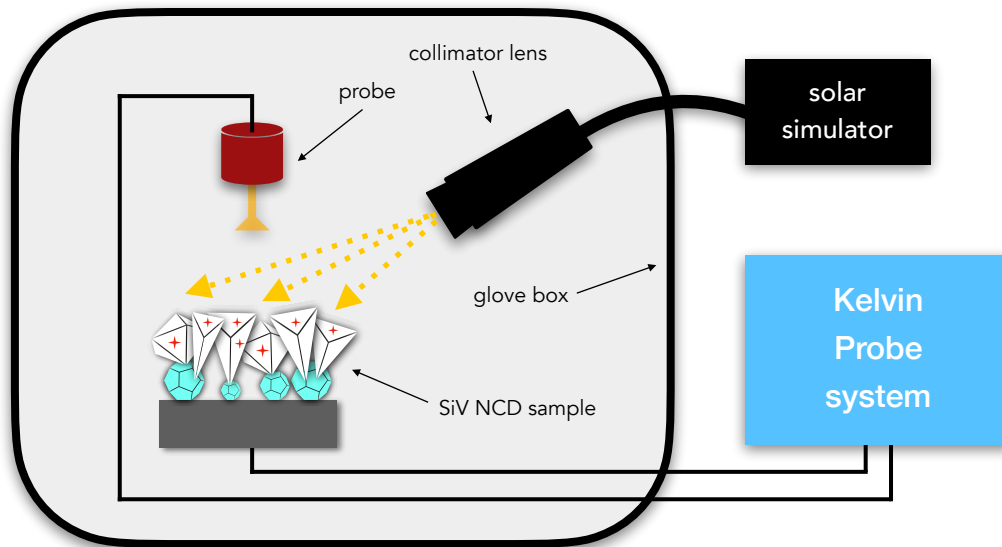

Figure 9. Scheme of the proposed experiment setup.

The experiment employed the scanning Kelvin probe method (KP Technology, UK) for CPD measurements [1]. The grounded steel probe, featuring a 2 mm diameter tip, was positioned inside a glove box with impermeable sides to light, ensuring complete darkness [1]. A solar simulator (class AAA solar simulator HAL-C100, Asahi Spectra, Japan) with a wide spectrum (400-1100 nm), simulating sunlight, was selected as the light source [1]. The simulator, equipped with an AM 1.5G filter, had its collimator lens also placed in the glove box (Figure 10). Measurements were done in a light-dark-light cycle, with the solar simulator manually switched on and off. To ensure stabilised charge, samples were illuminated for 7 minutes before CPD measurement, timed by a stopwatch. Subsequently, a continuous series of 750 points was recorded, with 250 points for each stage of the cycle, corresponding to 3 minutes each.

The obtained CPD data for each sample were recalculated to work function values using the following equation,

$$\mathrm{WF_{sample}} = \left(\mathrm{CPD_{sample}} - \mathrm{CPD_{ref}} \right) \cdot 10^{-3} + \mathrm{WF_{ref}} \tag{1}$$

where $\mathrm{WF_{sample}}$ is work function of the sample, $\mathrm{CPD_{sample}}$ is contact potential difference of the sample, $\mathrm{CPD_{ref}}$ is contact potential difference of a reference and $\mathrm{WF_{ref}}$ is work function of reference [1]. For reference, an Au reference sample provided by KP Technology was used [1]. Same sample served as a calibration before each set of measurements.
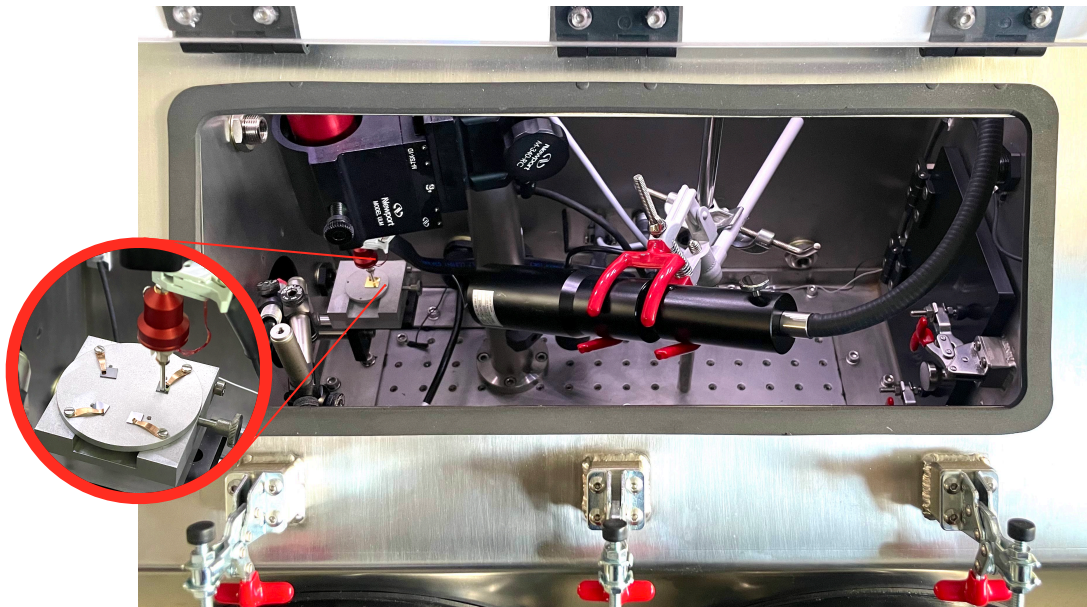

Figure 10. Photography of the setup is shown from the top, providing a view through the doors of the glovebox. The SKP probe with samples is positioned on the left, while the collimator lens is directed towards the measured point. A closer picture reveals mounted samples, prepared and ready for measurement.

Photovoltage was calculated using the following equation,

$$PV_{sample} = \overline{CPD}_{dark} - \overline{CPD}_{light} \tag{2}$$

where PV_{sample} is the photovoltage of the sample, $\overline{CPD}_{dark}$ is mean value of contact potential in dark phase and $\overline{CPD}_{light}$ is contact potential under illumination. To eliminate kinetic effects, if CPD was drifting in any of the phase, reduced number of values was used for calculation, using only values close to the switching point of the phases (light-dark).

PART III

Results and Discussion

9. Results

In the proposed experiment from the previous chapter, I measured the contact potential difference (CPD) of seven samples with varying thicknesses on both studied surface terminations, hydrogen-termination and oxygen-termination, respectively. The obtained values were recalculated to the work function using equation 1 and visualised in graphs (refer to Figure 11). The measurements were conducted in light-dark-light cycles, as illustrated in the graphs with a yellow background for the light phase and a grey background for the dark phase.
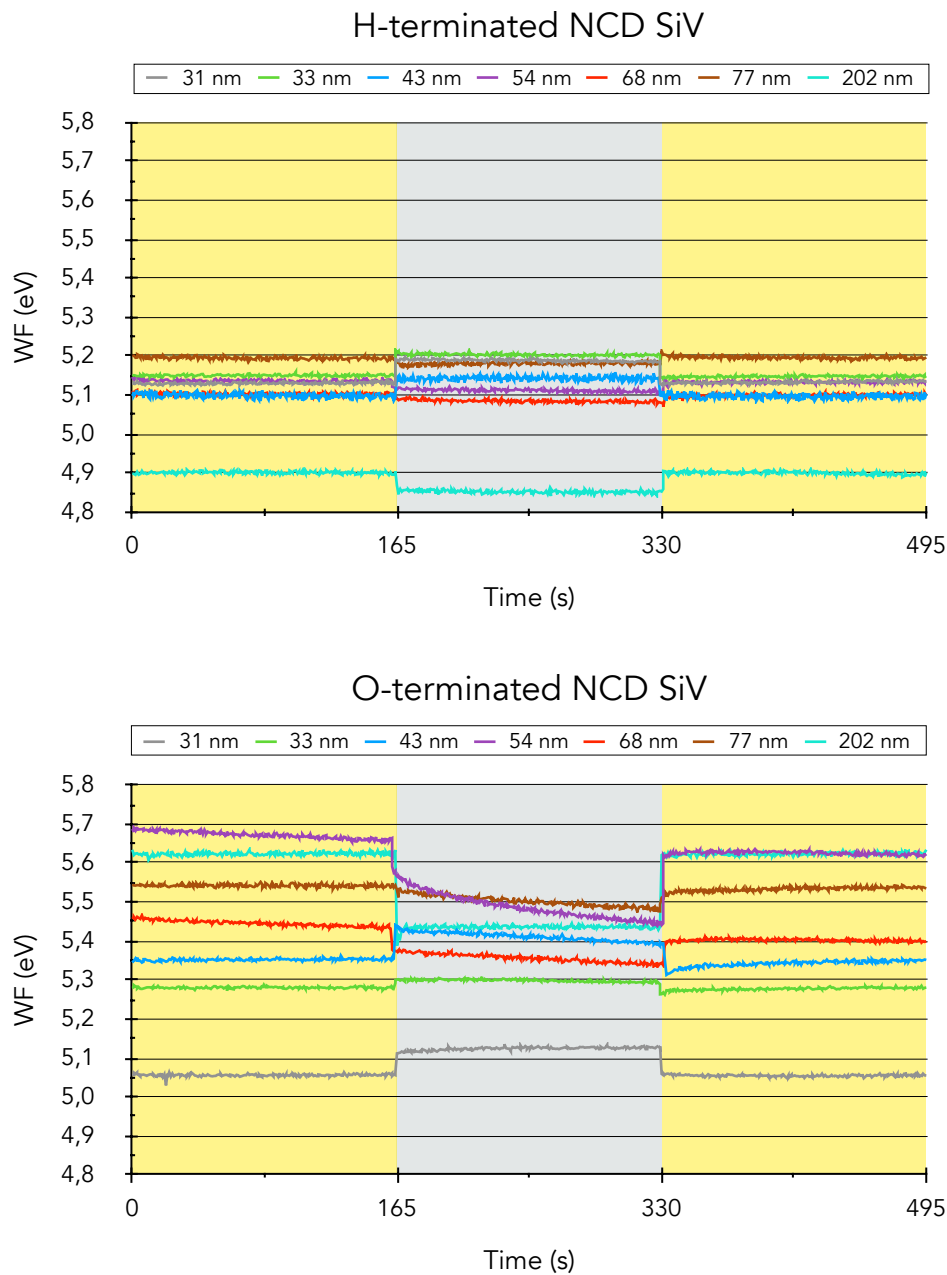
H-terminated NCD SiV

O-terminated NCD SiV

Figure 11. The measured work function values are for samples with different thicknesses and various surface terminations. In the graphs, the background colours represent the light-dark-light cycle, with yellow indicating the light phase and grey indicating the dark phase [1].

The measured values underwent further evaluation by determining the work function (WF) during the dark phase and generated photovoltage for each sample based on its thickness and surface termination. The work function was calculated as the average value when the illumination was turned off, with the addition of standard deviation. Photovoltage (PV) was computed using equation 2, also with the addition of combined standard deviation for difference. To enhance visualisation, the data are presented in graphs, with the average nucleation layer shown in grey, accompanied by trend lines serving as guiding aids for better orientation. Additionally, a table with values is provided in Table A.2. in the Appendices chapter.
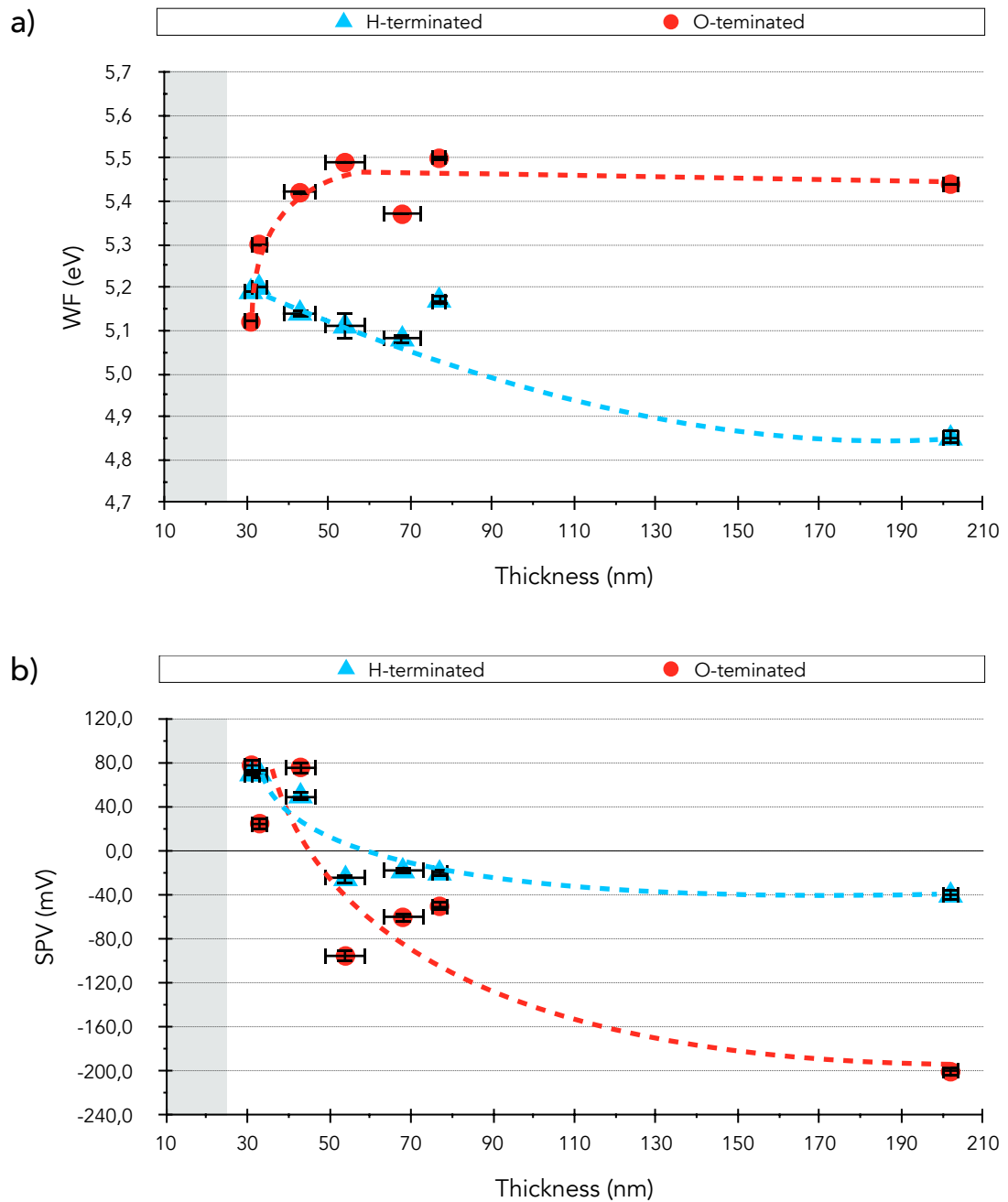

Figure 12. Graphs of a) average work function and b) surface photovoltage as function of thickness of SiV NCD layer for different surface modulations. Grey area representing nucleation layer, and trend lines acting as a visualisation of tendencies [1].

10. Discussion

Work function values in Figure 11 exhibit visible changes during a light-dark-light cycle. Values in the dark are considered as intrinsic properties of the sample, coming from its termination, NCD layer thickness, and potential electrostatic charge accumulation [1]. Illumination induces changes in work function, reflected in the generated photovoltage [5]. The recorded data over time provide insights into the kinetic behaviour of the surface potential [1,44].

H-terminated samples demonstrate more stable work function profiles, less prone to drifting, compared to O-terminated ones where drifting is observable during light-dark transitions. Drifting may be associated with sample discharge/charge [1]. Generally, samples under illumination remain stable, indicating successful supersaturation before and after the dark phase.

When WF work function under illumination is lower than in dark mode, positive generated photovoltage PV promotes a positive net charge on the surface. Conversely, higher work function under illumination results in negative generated photovoltage PV, yielding a negative net charge on the sample.

Data from light-dark-light cycles are presented in Figure 12, illustrating potential profiles for work function WF and photovoltage PV as functions of total thickness and surface chemistry. The nucleation layer is highlighted in grey for better visualisation, typically within the 15-25 nm range [12]. Figure 12a showcases typical values for samples with different surface chemistries. For O-terminated samples, work function increases with thickness, while for H-terminated samples, it decreases. Work function values stabilise/saturate for layers above 80 nm, corresponding to known bulk diamond work function values based on termination (4,9 eV for hydrogenated and 5,5 eV for oxygenated surfaces) [25,34].

Major variations occur for thicknesses below 90 nm, indicating layer specific behaviour different from bulk properties. Noteworthy is the variance in H-terminated work function (WF), around 0,1 eV for low thicknesses. A visible plateau phase in the thinnest samples can be explained by a p-type surface conduction layer (SCL) formed by accumulated positively charged holes due to hydrogen termination, as suggested by various studies [1,5]. This is supported by the fact that this WF value is the highest for this type of surface chemistry and is absent in oxidised samples. The behaviour in the thinnest H samples can be attributed to the effect of grain boundaries, serving as electron traps [5,23,41,46]. Grain boundaries have been more present on lower thickness samples due to not yet fully grown uniform layer covering whole substrate. The obtained WF values, dependent on thickness and surface chemistry, correspond with findings in other studies [1,5,34,44].

Photovoltage (PV) profiles in Figure 12b exhibit a decreasing trend with increasing thickness for both surface terminations. Low thickness samples (30-43 nm) generate positive PV, while thicker layers (more than 43 nm) yield negative PV, switching polarity around 60 nm for H-terminated and 45 nm for O-terminated. Further thickness increase leads to overall PV reduction, stabilising at around −50 mV for H-terminated and −200 mV for O-terminated samples. These negative values for thick samples correspond with findings for bulk diamond layers in other studies [5,44].

Based on these results and existing studies, a band diagram for PV generation can be proposed.

Rezek et al. presented a study measuring CPD between the surface of hydrogenated diamond and golden contacts [25]. The result indicated the same work function (WF) across both materials, revealing that the Fermi level is positioned below the valence band maximum (VBM) in the surface area of H-terminated NCD, approximately 0,7 eV below VBM. This suggests an upward bending of the bands, indicating electron depletion in this region due to negative electron affinity, leading to the formation of a p-type surface conduction layer (SCL) consisting of holes [1,5,45]. According to the work by Stehlík et al., the thickness of the SCL is considered to be 10 nm [5]. Experiments showed that photoluminescence (PL) is quenched for layers <10 nm, implying that excited electrons cannot reach SiV states as they recombine with holes in the SCL [1]. The potential mechanism for the formation of such a layer was initially considered as the transformation of SiV^- centres to neutrally charged SiV^0 near the surface, but no photoluminescence at 946 nm was observed [5]. A more likely mechanism involves electrons excited by illumination to SiV centres, are drawn towards SiV centres of lower energies, creating holes that accumulate toward the surface, resulting in a positive charge, as illustrated in Figure 13 [1,5,45]. The reason for this accumulation may be attributed to surface states or the presence of sp^2 carbon phases due to grain boundaries [1,5,41].

For thicknesses above 10 nm, excited SiV centres continue to generate holes, contributing to a positive charge until the SiV excited state drops below the Fermi level, estimated to be around double the thickness of the surface conduction layer (SCL), approximately 20 nm [1]. In the band diagram, this positive contribution of SiV states is marked as (SPV+). Further increases in layer thickness allow the excited states of SiV to become occupied, contributing with a negative charge (SPV−) [1]. At this depth, photoluminescence also increases, allowing radiative recombinations. Continued negative contributions result in a neutral net charge at a layer thickness corresponding to 40 nm, four times the thickness of the SCL [1]. This thickness is considered as the boundary between surface-controllable SiV centres and bulk SiV centres [1]. In Figure 12b, this thickness marks the point where photovoltage (PV) switches polarity, corresponding to around 55-65 nm of total thickness, considering the nucleation layer variance of 15-25 nm [1]. The negative contribution of deeper SiV centres continues until PV stabilises.

A band diagram for O-terminated samples is also proposed, as illustrated in Figure 13. Stehlík et al. observed photoluminescence (PL) on a O-terminated sample with a thickness of 10 nm, suggesting that SiV excited states on such samples are below the Fermi level [1,5]. The bands are similarly bent upwards, but the Fermi level is pinned at a value of 1,8-2,2 eV above the valence band maximum (VBM) due to surface states, as noted by Stehlík et al. [5,24]. These surface states are more prevalent than on hydrogenated samples and function as hole traps [5]. The band bending promotes the trapping of photoexcited holes, allowing them to move toward the surface more easily, resulting in a positive charge for thin layers [1,5]. The thickness of the positively contributing layer (SPV+) in the graph can be described as the band bending depth [1]. As the layer thickness increases, excited SiV states contribute (SPV−) negatively, reaching a neutral net charge at approximately double the band bending depth [1]. The thickness at which photovoltage (PV) changes polarity is determined in Figure 12b, around 45 nm of total thickness, resulting in a band bending depth of 10 nm. Further contribution leads to stabilisation at around −200 mV.
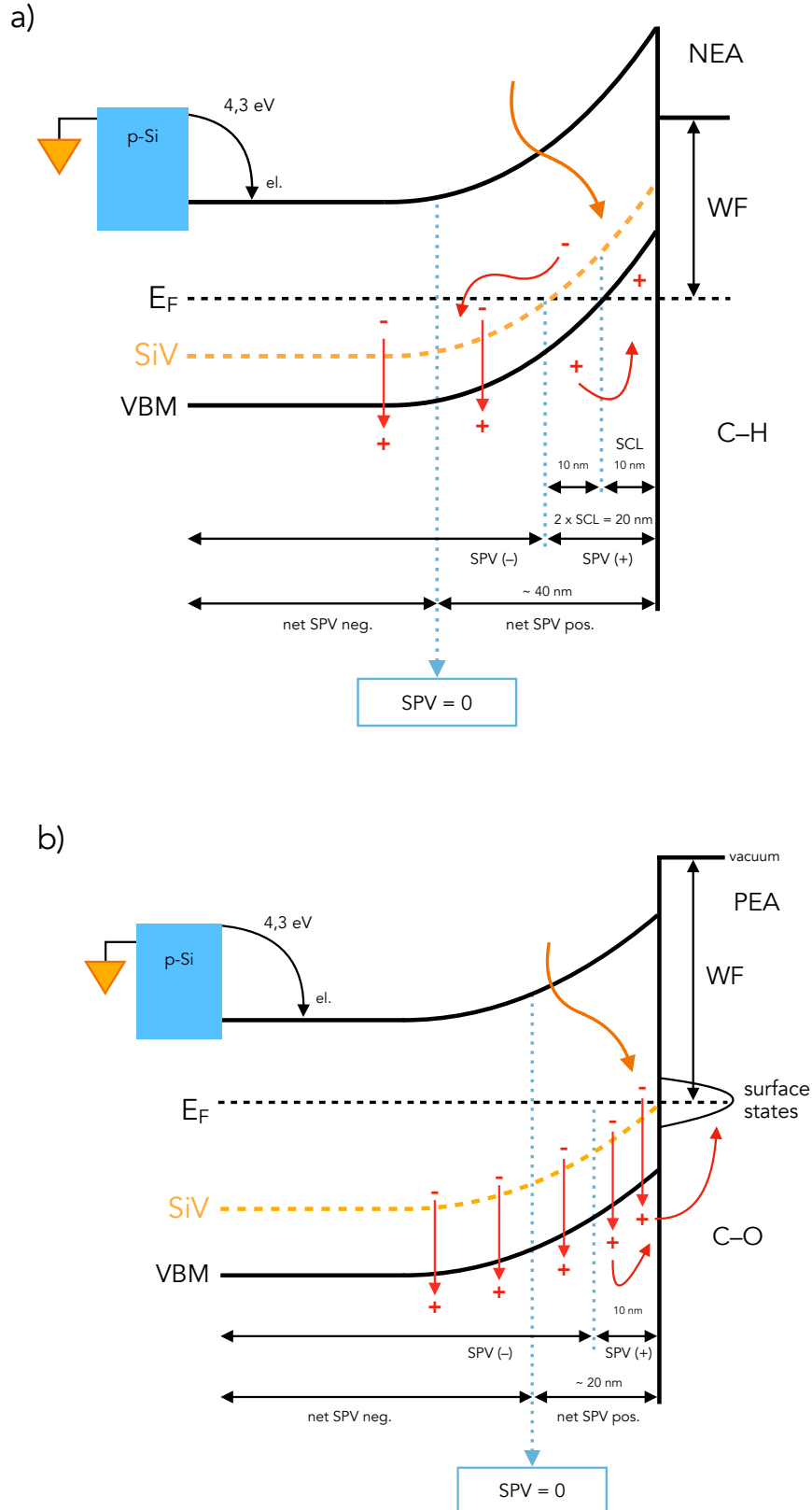
a)

NEA

p-Si   4,3 eV

el.

WF

E_F

SiV

VBM

−

−

+

+

−

−

+

+

+

SCL

10 nm   10 nm

2 x SCL = 20 nm

SPV (–)   SPV (+)

~ 40 nm

net SPV neg.   net SPV pos.

C–H

SPV = 0

b)

vacuum

PEA

p-Si   4,3 eV

el.

WF

surface states

E_F

SiV

VBM

−

−

+

+

−

−

+

+

−

−

+

+

−

−

+

+

C–O

10 nm

SPV (–)   SPV (+)

~ 20 nm

net SPV neg.   net SPV pos.

SPV = 0

Figure 13. Proposed band diagrams for a) H-terminated and b) O-terminated SiV NCD samples for PV generation and polarity switching, dependent on thickness. Dark orange arrow represents illumination, red arrows represent excitation and movement of holes. [1,5,44]

The proposed mechanism above can enhance our understanding of the relationship between bulk SiV centres and those SiV centres situated in sub-surface areas [46]. However, detailed mechanisms still need to be evaluated. The principles and explanations utilised in this context do not account for all elements that might influence the actual mechanism.

Polycrystalline diamond defects, including grain boundaries and sp^2-related defects, are considered as important for the light emission efficiency of SiV centres, as indicated by several studies [23,33,41]. These defects have a significant impact on photoluminescence (PL). Additionally, the silicon-diamond bottom junction and the potential influence of deep level traps may also play a role [1]. However, these elements have not been extensively integrated into the existing theory PV generation.

Improving conditions during Kelvin probe measurements can be also important, as some studies indicate that the hydrophilic nature of the O-terminated surface might cause a potential-masking effect due to adsorbed water molecules [29,42]. For instance, Stehlík et al. conducted measurements in an inert atmosphere and annealed the samples before the measurement to minimise the impact of surface dipoles caused by water molecules [5,29,42]. Achieving such conditions for future measurements is possible, given the use of a glove box in the experiment, which allows for the use of dry nitrogen to ensure an inert and humidity-free atmosphere [5]. Future experiments may include photoluminescence (PL) measurements as an important method for studying surface chemistry and photovoltage of SiV NCD samples. Additionally, the use of tunable laser illumination (400-800 nm) could be considered [1].

It is important to note, that the proposed mechanisms above are based on the results and measurements I performed in this work.. Kuliček et al. have published a paper incorporating these results into a more complex experiment, yielding a more precise mechanism and incorporating additional quantities [1]. Their work includes supplementary measurements such as photoluminescence (PL) measurements, Raman spectroscopy, and roughness measurements. The published paper is provided in the Appendices chapter, B.1.

11. Conclusion

In this thesis, I analysed polycrystalline thin NCD films with SiV centres, varying in thickness and featuring either hydrogen-terminated or oxygen-terminated surfaces. Thickness measurements, ranging from 31 to 200 nm, were conducted using SEM and reflectance interferometry. I proposed and performed an experiment to determine CPD values during a light-dark-light cycle using the Kelvin probe method.

Results were transformed into work function (WF) and photovoltage (PV). WF values exhibit dependency on sample thickness and surface chemistry. For H-terminated samples, the work function decreases with thickness, while for O-terminated samples, values increases. Both terminations reach values typical for bulk diamond at the highest thickness.

Surface photovoltage also displays dependency on sample thickness, with a consistent decrease in generated PV values for both surface terminations. A change in polarity occurs for samples with a total thickness exceeding 50 nm, setting the boundary between surface-controllable SiV centres and bulk SiV centres.

Based on these results, I proposed band diagrams of photovoltage generation for each surface chemistry, that help with better understanding of SiV based processes in diamond layers. This study opens the potential use of NCD SiV layers in biomedical sensing or energy harvesting applications.

References

1. KULIČEK, Jaroslav; MAREK, Maxmilian; KUMAR, Nirmal; FAIT, Jan; POTOCKÝ, Štěpán et al. Kelvin Probe Characterization of Nanocrystalline Diamond Films with SiV Centres as Function of Thickness. Online. Physica status solidi (a). 2023. ISSN 1862-6300. Dostupné z: https://doi.org/10.1002/pssa.202300459. [cit. 2023-12-11].

2. LI, Ke; ZHOU, Yu; RASMITA, A.; AHARONOVICH, I. a GAO, W. B. Nonblinking Emitters with Nearly Lifetime-Limited Linewidths in CVD Nanodiamonds. Online. Physical Review Applied. 2016, roč. 6, č. 2. ISSN 2331-7019. Dostupné z: https://doi.org/10.1103/PhysRevApplied.6.024010. [cit. 2023-12-11].

3. AHARONOVICH, I; CASTELLETTO, S; SIMPSON, D A; SU, C-H; GREENTREE, A D et al. Diamond-based single-photon emitters. Online. Reports on Progress in Physics. 2011, roč. 74, č. 7. ISSN 0034-4885. Dostupné z: https://doi.org/10.1088/0034-4885/74/7/076501. [cit. 2023-12-11].

4. STEHLIK, Stepan; VARGA, Marian; STENCLOVA, Pavla; ONDIC, Lukas; LEDINSKY, Martin et al. Ultrathin Nanocrystalline Diamond Films with Silicon Vacancy Colour Centres via Seeding by 2 nm Detonation Nanodiamonds. Online. 2017, roč. 9, č. 44, s. 38842-38853. ISSN 1944-8244. Dostupné z: https://doi.org/10.1021/acsami.7b14436. [cit. 2023-12-11].

5. STEHLIK, Stepan; ONDIC, Lukas; VARGA, Marian; FAIT, Jan; ARTEMENKO, Anna et al. Silicon-Vacancy Centres in Ultra-Thin Nanocrystalline Diamond Films. Online. Micromachines. 2018, roč. 9, č. 6. ISSN 2072-666X. Dostupné z: https://doi.org/10.3390/mi9060281. [cit. 2023-12-11].

6. ASAHI SPECTRA. Solar Simulator (100-100nm) HAL-C100. User Manual. 2017.

7. DOMONKOS, Mária. Micro- and nanoscale diamond structuring. Doctoral Thesis. Prague: Czech Technical University in Prague, 2018.

8. PROCHÁZKA, Václav. Biosensors Based on Nanocrystalline Diamond. Doctoral Thesis. Prague: Czech Technical University in Prague, 2022.

9. FAIT, Jan. Fabrication and Characterisation of Diamond Photonic Structures. Doctoral Thesis. Prague: Czech Technical University in Prague, 2020.

10. WILLIAMS, Oliver A.; DOUHÉRET, Olivier; DAENEN, Michael; HAENEN, Ken; ŌSAWA, Eiji et al. Enhanced diamond nucleation on monodispersed nanocrystalline diamond. Online. Chemical Physics Letters. 2007, roč. 445, č. 4-6, s. 255-258. ISSN 00092614. Dostupné z: https://doi.org/10.1016/j.cplett.2007.07.091. [cit. 2023-12-11].

11. NEU, Elke; STEINMETZ, David; RIEDRICH-MÖLLER, Janine; GSELL, Stefan; FISCHER, Martin et al. Single photon emission from silicon-vacancy colour centres in chemical vapour deposition nano-diamonds on iridium. Online. New Journal of Physics. 2011, roč. 13, č. 2. ISSN 1367-2630. Dostupné z: https://doi.org/10.1088/1367-2630/13/2/025012. [cit. 2023-12-11].

12. KROMKA, Alexander; REZEK, Bohuslav; REMES, Zdenek; MICHALKA, Miroslav; LEDINSKY, Martin et al. Formation of Continuous Nanocrystalline Diamond Layers on Glass and Silicon at Low Temperatures. Online. Chemical Vapor Deposition. 2008, roč. 14, č. 7-8, s. 181-186. ISSN 0948-1907. Dostupné z: https://doi.org/10.1002/cvde.200706662. [cit. 2023-12-11].

13. PABLO PENNISI, Cristian a ALCAIDE, María. Nanocrystalline Diamond Films for Biomedical Applications. Online. Frontiers in Biomaterials. 2014, s. 70-100. ISBN 9781608058761. Dostupné z: https://doi.org/10.2174/9781608058761114010006. [cit. 2023-12-11].

14. VLASOV, Igor I.; BARNARD, Amanda S.; RALCHENKO, Victor G.; LEBEDEV, Oleg I.; KANZYUBA, Mikhail V. et al. Nanodiamond Photoemitters Based on Strong Narrow-Band Luminescence from Silicon-Vacancy Defects. Online. Advanced Materials. 2009, roč. 21, č. 7, s. 808-812. ISSN 0935-9648. Dostupné z: https://doi.org/10.1002/adma.200802160. [cit. 2023-12-11].

15. RADULASKI, Marina; ZHANG, Jingyuan Linda; TZENG, Yan-Kai; LAGOUDAKIS, Konstantinos G.; ISHIWATA, Hitoshi et al. Nanodiamond Integration with Photonic Devices. Online. 2019, roč. 13, č. 8. ISSN 1863-8880. Dostupné z: https://doi.org/10.1002/lpor.201800316. [cit. 2023-12-11].

16. LIU, Weina; ALAM, Md Noor A.; LIU, Yan; AGAFONOV, Viatcheslav N.; QI, Haoyuan et al. Silicon-Vacancy Nanodiamonds as High Performance Near-Infrared Emitters for Live-Cell Dual-Colour Imaging and Thermometry. Online. Nano Letters. 2022, roč. 22, č. 7, s. 2881-2888. ISSN 1530-6984. Dostupné z: https://doi.org/10.1021/acs.nanolett.2c00040. [cit. 2023-12-11].

17. BRADAC, Carlo; GAO, Weibo; FORNERIS, Jacopo; TRUSHEIM, Matthew E. a AHARONOVICH, Igor. Quantum nanophotonics with group IV defects in diamond. Online. Nature Communications. 2019, roč. 10, č. 1. ISSN 2041-1723. Dostupné z: https://doi.org/10.1038/s41467-019-13332-w. [cit. 2023-12-11].

18. D'HAENENS-JOHANSSON, U. F. S.; EDMONDS, A. M.; GREEN, B. L.; NEWTON, M. E.; DAVIES, G. et al. Optical properties of the neutral silicon split-vacancy centre in diamond. Online. Physical Review B. 2011, roč. 84, č. 24. ISSN 1098-0121. Dostupné z: https://doi.org/10.1103/PhysRevB.84.245208. [cit. 2023-12-11].

19. ROGERS, Lachlan J.; JAHNKE, Kay D.; DOHERTY, Marcus W.; DIETRICH, Andreas; MCGUINNESS, Liam P. et al. Electronic structure of the negatively charged silicon-vacancy centre in diamond. Online. Physical Review B. 2014, roč. 89, č. 23. ISSN 1098-0121. Dostupné z: https://doi.org/10.1103/PhysRevB.89.235101. [cit. 2023-12-11].

20. GALI, Adam a MAZE, Jeronimo R. Ab initio study of the split silicon-vacancy defect in diamond: Electronic structure and related properties. Online. Physical Review B. 2013, roč. 88, č. 23. ISSN 1098-0121. Dostupné z: https://doi.org/10.1103/PhysRevB.88.235205. [cit. 2023-12-11].

21. JAHNKE, Kay D; SIPAHIGIL, Alp; BINDER, Jan M; DOHERTY, Marcus W; METSCH, Mathias et al. Electron–phonon processes of the silicon-vacancy centre in diamond. Online. New Journal of Physics. 2015, roč. 17, č. 4. ISSN 1367-2630. Dostupné z: https://doi.org/10.1088/1367-2630/17/4/043011. [cit. 2023-12-11].

22. HUGHES, A. E. ZERO-PHONON TRANSITIONS AND VIBRATIONAL STRUCTURE. Online. Le Journal de Physique Colloques. 1967, roč. 28, č. C4, s. C4-55-C4-65. ISSN 0449-1947. Dostupné z: https://doi.org/10.1051/jphyscol:1967408. [cit. 2023-12-11].

23. TROJÁNEK, František; HAMRÁČEK, Karol; HANÁK, Martin; VARGA, Marián; KROMKA, Alexander et al. Light emission dynamics of silicon vacancy centres in a polycrystalline diamond thin film. Online. Nanoscale. 2023, roč. 15, č. 6, s. 2734-2738. ISSN 2040-3364. Dostupné z: https://doi.org/10.1039/D2NR05470A. [cit. 2023-12-11].

24. ITOH, Yutaka; SUMIKAWA, Yu; UMEZAWA, Hitoshi a KAWARADA, Hiroshi. Trapping mechanism on oxygen-terminated diamond surfaces. Online. Applied Physics Letters. 2006, roč. 89, č. 20. ISSN 0003-6951. Dostupné z: https://doi.org/10.1063/1.2387983. [cit. 2023-12-11].

25. REZEK, B. a NEBEL, C.E. Kelvin force microscopy on diamond surfaces and devices. Online. Diamond and Related Materials. 2005, roč. 14, č. 3-7, s. 466-469. ISSN 09259635. Dostupné z: https://doi.org/10.1016/j.diamond.2005.01.041. [cit. 2023-12-11].

26. KROMKA, A.; POTOCKÝ, Š.; ČERMÁK, J.; REZEK, B.; POTMĚŠIL, J. et al. Early stage of diamond growth at low temperature. Online. Diamond and Related Materials. 2008, roč. 17, č. 7-10, s. 1252-1255. ISSN 09259635. Dostupné z: https://doi.org/10.1016/j.diamond.2008.03.035. [cit. 2023-12-11].

27. FAIT, Jan; VARGA, Marián; HRUŠKA, Karel; REMEŠ, Zdeněk; JURKA, Vlastimil et al. Maximized vertical photoluminescence from optical material with losses employing resonant excitation and extraction of photonic crystal modes. Online. Nanophotonics. 2019, roč. 8, č. 6, s. 1041-1050. ISSN 2192-8614. Dostupné z: https://doi.org/10.1515/nanoph-2019-0042. [cit. 2023-12-11].

28. POTOCKÝ, Štěpán; IŽÁK, Tibor; VARGA, Marian a KROMKA, Alexander. Influence of gas chemistry on Si-V colour centres in diamond films. Online. Physica status solidi (b). 2015, roč. 252, č. 11, s. 2580-2584. ISSN 03701972. Dostupné z: https://doi.org/10.1002/pssb.201552222. [cit. 2023-12-11].

29. STEHLIK, S.; GLATZEL, T.; PICHOT, V.; PAWLAK, R.; MEYER, E. et al. Water interaction with hydrogenated and oxidized detonation nanodiamonds — Microscopic and spectroscopic analyses. Online. Diamond and Related Materials. 2016, roč. 63, s. 97-102. ISSN 09259635. Dostupné z: https://doi.org/10.1016/j.diamond.2015.08.016. [cit. 2023-12-11].

30. YANG, Bing; YU, Biao; LI, Haining; HUANG, Nan; LIU, Lusheng et al. Enhanced and switchable silicon-vacancy photoluminescence in air-annealed nanocrystalline diamond films. Online. Carbon. 2020, roč. 156, s. 242-252. ISSN 00086223. Dostupné z: https://doi.org/10.1016/j.carbon.2019.09.054. [cit. 2023-12-11].

31. EDLER, Frederik; MICCOLI, Ilio; PFNÜR, Herbert a TEGENKAMP, Christoph. Space charge layer effects in silicon studied by in situ surface transport. Online. Journal of Physics: Condensed Matter. 2019, roč. 31, č. 21. ISSN 0953-8984. Dostupné z: https://doi.org/10.1088/1361-648X/ab094e. [cit. 2023-12-11].

32. MAIER, F.; RIEDEL, M.; MANTEL, B.; RISTEIN, J. a LEY, L. Origin of Surface Conductivity in Diamond. Online. Physical Review Letters. 2000, roč. 85, č. 16, s. 3472-3475. ISSN 0031-9007. Dostupné z: https://doi.org/10.1103/PhysRevLett.85.3472. [cit. 2023-12-11].

33. MAKINO, Yuto; MAHIKO, Tomoaki; LIU, Ming; TSURUI, Akihiko; YOSHIKAWA, Taro et al. Straightforward synthesis of silicon vacancy (SiV) centre-containing single-digit nanometer nanodiamonds via detonation process. Online. Diamond and Related Materials. 2021, roč. 112. ISSN 09259635. Dostupné z: https://doi.org/10.1016/j.diamond.2021.108248. [cit. 2023-12-11].

34. MAIER, F.; RISTEIN, J. a LEY, L. Electron affinity of plasma-hydrogenated and chemically oxidized diamond (100) surfaces. Online. Physical Review B. 2001, roč. 64, č. 16. ISSN 0163-1829. Dostupné z: https://doi.org/10.1103/PhysRevB.64.165411. [cit. 2023-12-11].

35. FAKLARIS, Orestis; GARROT, Damien; JOSHI, Vandana; DRUON, Frédéric; BOUDOU, Jean-Paul et al. Detection of Single Photoluminescent Diamond Nanoparticles in Cells and Study of the Internalization Pathway. Online. Small. 2008, roč. 4, č. 12, s. 2236-2239. ISSN 1613-6810. Dostupné z: https://doi.org/10.1002/smll.200800655. [cit. 2023-12-11].

36. MOHAN, Nitin; TZENG, Yan-Kai; YANG, Liling; CHEN, Yi-Ying; HUI, Yuen Yung et al. Sub-20-nm Fluorescent Nanodiamonds as Photostable Biolabels and Fluorescence Resonance Energy Transfer Donors. Online. Advanced Materials. 2010, roč. 22, č. 7, s. 843-847. ISSN 0935-9648. Dostupné z: https://doi.org/10.1002/adma.200901596. [cit. 2023-12-11].

37. MÜLLER, Tina; HEPP, Christian; PINGAULT, Benjamin; NEU, Elke; GSELL, Stefan et al. Optical signatures of silicon-vacancy spins in diamond. Online. Nature Communications. 2014, roč. 5, č. 1. ISSN 2041-1723. Dostupné z: https://doi.org/10.1038/ncomms4328. [cit. 2023-12-11].

38. MARTINSEN, Ørjan G. a HEISKANEN, Arto. Electrodes. Online. Bioimpedance and Bioelectricity Basics. 2023, s. 175-248. ISBN 9780128191071. Dostupné z: https://doi.org/10.1016/B978-0-12-819107-1.00005-4. [cit. 2023-12-11].

39. KP TECHNOLOGY. Scanning Kelvin Probe User Manual: Manual Version SKP KP 5.0. User manual.

40. KAHN, Antoine. Fermi level, work function and vacuum level. Online. Materials Horizons. 2016, roč. 3, č. 1, s. 7-10. ISSN 2051-6347. Dostupné z: https://doi.org/10.1039/C5MH00160A. [cit. 2023-12-11].

41. HARNIMAN, Robert L.; FOX, Oliver J.L.; JANSSEN, Wiebke; DRIJKONINGEN, Sien; HAENEN, Ken et al. Direct observation of electron emission from grain boundaries in CVD diamond by PeakForce-controlled tunnelling atomic force microscopy. Online. Carbon. 2015, roč. 94, s. 386-395. ISSN 00086223. Dostupné z: https://doi.org/10.1016/j.carbon.2015.06.082. [cit. 2023-12-11].

42. LAY, J.H.; O'DONNELL, K.M. a MAY, P.W. Workfunction variation across surface of an H-terminated diamond film measured using Kelvin probe force microscopy. Online. Chemical Physics Letters. 2011, roč. 515, č. 1-3, s. 151-154. ISSN 00092614. Dostupné z: https://doi.org/10.1016/j.cplett.2011.09.023. [cit. 2023-12-11].

43. KROMKA, A.; POTOCKÝ, Š.; ČERMÁK, J.; REZEK, B.; POTMĚŠIL, J. et al. Early stage of diamond growth at low temperature. Online. Diamond and Related Materials. 2008, roč. 17, č. 7-10, s. 1252-1255. ISSN 09259635. Dostupné z: https://doi.org/10.1016/j.diamond.2008.03.035. [cit. 2023-12-11].

44. REZEK, B.; NEBEL, C.E. a STUTZMANN, M. Hydrogenated diamond surfaces studied by atomic and Kelvin force microscopy. Online. Diamond and Related Materials. 2004, roč. 13, č. 4-8, s. 740-745. ISSN 09259635. Dostupné z: https://doi.org/10.1016/j.diamond.2003.11.051. [cit. 2023-12-11].

45. REZEK, B.; SAUERER, C.; NEBEL, C. E.; STUTZMANN, M.; RISTEIN, J. et al. Fermi level on hydrogen terminated diamond surfaces. Online. Applied Physics Letters. 2003, roč. 82, č. 14, s. 2266-2268. ISSN 0003-6951. Dostupné z: https://doi.org/10.1063/1.1564293. [cit. 2023-12-11].

46. VERVENIOTIS, E.; KROMKA, A.; LEDINSKÝ, M. a REZEK, B. How nanocrystalline diamond films become charged in nanoscale. Online. Diamond and Related Materials. 2012, roč. 24, s. 39-43. ISSN 09259635. Dostupné z: https://doi.org/10.1016/j.diamond.2011.10.002. [cit. 2023-12-11].

Appendices

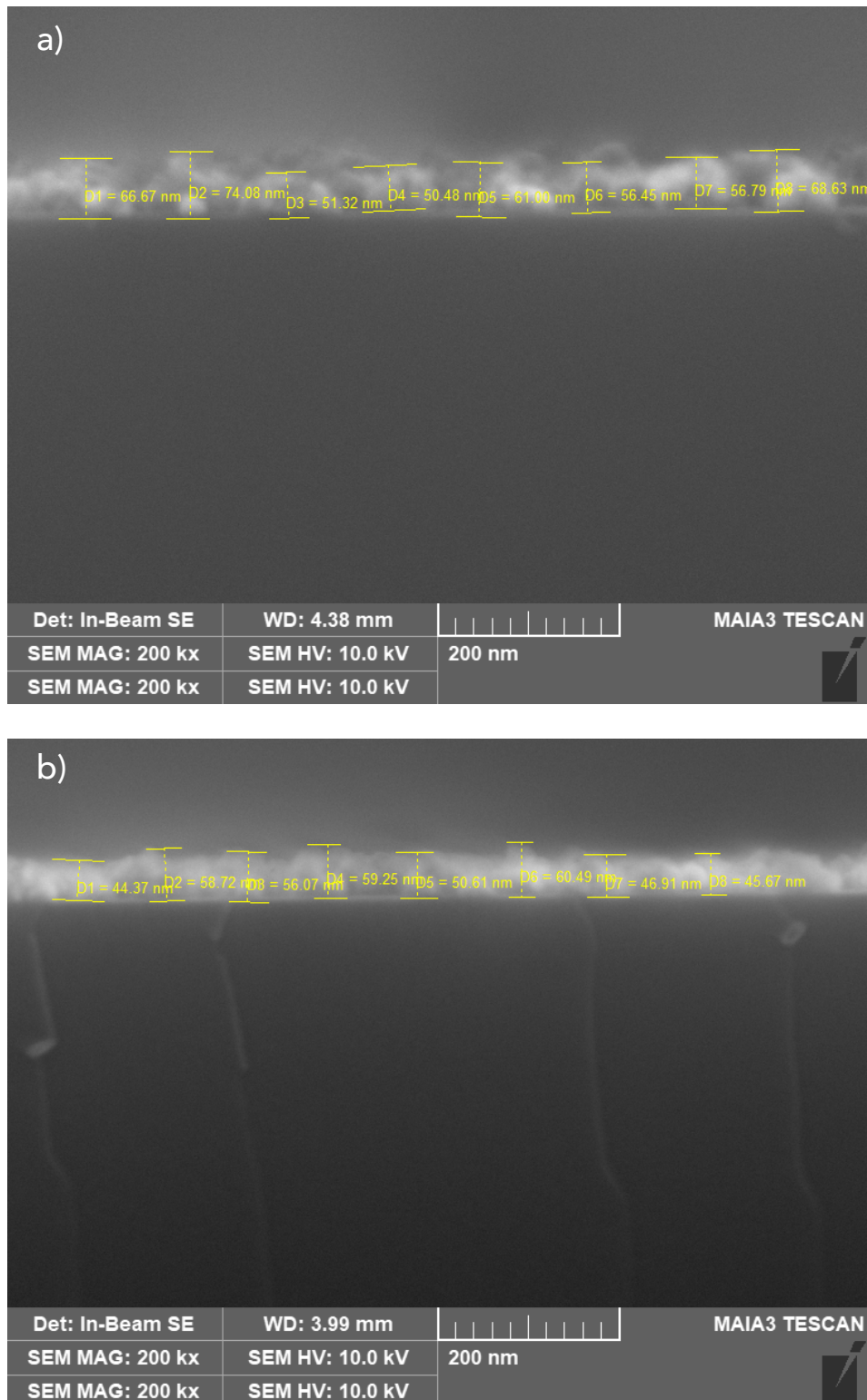## List of Appendices

A.1. SEM measurement image

Figure A.1. SEM images with displayed measurement points for a) H-terminated and b) O-terminated samples.

A.2. WF and PV data table

Table A.2.1. Obtained values for H-terminated samples

Sample	Total thicknness (nm)	WF_{sample} (eV)	$\overline{\text{CPD}}_{light}$ (mV)	$\overline{\text{CPD}}_{dark}$ (mV)	PV_{sample} (mV)
1	31 ± 1	5,19 ± 0,00	92,9 ± 2,7	162,5 ± 3,4	69,6 ± 0,9
2	33 ± 2	5,20 ± 0,00	113,1 ± 2,4	181,0 ± 3,3	67,9 ± 0,9
3	43 ± 4	5,14 ± 0,01	61,6 ± 6,6	113,2 ± 7,9	51,6 ± 1,4
4	54 ± 5	5,11 ± 0,00	99,5 ± 3,5	74,3 ± 2,5	− 25,2 ± 0,8
5	68 ± 5	5,08 ± 0,00	65,3 ± 3,3	46,9 ± 1,6	− 18,4 ± 0,6
6	77 ± 2	5,17 ± 0,00	158,0 ± 3,9	134,9 ± 5,2	− 23,1 ± 1,2
7	202 ± 2	5,85 ± 0,00	122,0 ± 3,4	80,6 ± 8,5	− 41,4 ± 1,5

Table A.2.2. Obtained values for O-terminated samples

Sample	Total thicknness (nm)	WF_{sample} (eV)	$\overline{\text{CPD}}_{light}$ (mV)	$\overline{\text{CPD}}_{dark}$ (mV)	PV_{sample} (mV)
1	31 ± 1	5,12 ± 0,00	18,9 ± 3,1	96,9 ± 1,9	78,0 ± 0,7
2	33 ± 2	5,30 ± 0,00	243,5 ± 2,4	268,0 ± 1,8	24,7 ± 0,7
3	43 ± 4	5,42 ± 0,01	315,2 ± 2,9	392,0 ± 3,2	76,8 ± 0,9
4	54 ± 5	5,49 ± 0,03	635,4 ± 8,9	540,6 ± 4,4	− 94,8 ± 1,1
5	68 ± 5	5,37 ± 0,01	408,5 ± 7,2	347,1 ± 2,4	− 61,4 ± 0,8
6	77 ± 2	5,50 ± 0,01	505,4 ± 3,8	452,3 ± 9,2	− 53,1 ± 1,5
7	202 ± 2	5,44 ± 0,02	541,9 ± 4,5	336,7 ± 14,9	− 205,2 ± 1,9

Kelvin Probe Characterization of Nanocrystalline Diamond Films with SiV Centers as Function of Thickness

Jaroslav Kuliček,* Maxmilian Marek, Nirmal Kumar, Jan Fait, Štěpán Potocký, Štěpán Stehlík, Alexander Kromka, and Bohuslav Rezek

Optically active color centers in diamonds have been intensively studied due to their potential in photonics, energy harvesting, biosensing, and quantum computing. Silicon vacancy (SiV) center offers an advantage of suitable emission wavelength and narrow zero-phonon line at room temperature. Measurement of surface potential and photovoltage can provide better understanding of the physics and control of SiV light emission, such as charge states and charging effects. Herein, optoelectronic properties of nanocrystalline diamond films with SiV centers at different layer thicknesses (10–200 nm, controlled by the growth time) under ambient conditions are studied. Time-dependent measurements are performed in the light–dark–light cycle. Positive photovoltage arises on samples with SiV layer thicknesses below 55 nm on both H- and O-terminated surfaces. Above 55 nm the photovoltage switches to negative. This layer thickness thus represents a halfway boundary between surface-controllable and bulk SiV centers dominant contribution. A band diagram scheme explaining the photovoltage switching mechanism is provided.

1. Introduction

Unique properties of diamond, such as its high biocompatibility,[1,2] optical transparency,[3] and low chemical reactivity,[4] make it an attractive material for various applications. Among the different types of diamonds, nanocrystalline diamond (NCD) films have been widely investigated due to high mechanical strength,[5] low friction coefficient,[6,7] high thermal conductivity[8] as well as diverse thin film biosensing devices.[9–11]

J. Kuliček, M. Marek, N. Kumar, Š. Potocký, B. Rezek
Faculty of Electrical Engineering
Czech Technical University in Prague
Technická 2, 16627 Prague, Czech Republic
E-mail: kulicjar@fel.cvut.cz

J. Fait, Š. Stehlík, A. Kromka
Institute of Physics
Czech Academy of Sciences
Cukrovarnická 10, 16200 Prague, Czech Republic

One of the most promising applications of NCD is also in quantum technologies, where the material unique properties can be utilized for quantum computing, quantum sensing, and quantum communication.[12,13] In particular, the silicon vacancy (SiV) center in NCD has attracted significant attention due to its excellent optical and spin properties.[14] The SiV center is a point defect in the diamond lattice that consists of a substitutional silicon atom and a neighboring vacancy. The SiV center exhibits a sharp zero-phonon line (ZPL) at around 738 nm,[15] which makes it an attractive material for applications in sensing.

The SiV center in NCDs has several advantages over other color centers such as nitrogen vacancy (NV) in diamonds. Despite its shorter spin-coherence time, SiV center is more resistant to local crystal defects thanks to its inversion symmetry.[16] This allows placing SiV centers into nanophotonic cavities[17] or using centers located in nanodiamonds for quantum applications.[18] It also has a higher brightness,[19] which makes it easier to detect and manipulate. Furthermore, the SiV center has a narrow linewidth, which enables high-resolution spectroscopy.[20]

Changes in the color centers of SiV NCDs are mainly investigated by photoluminescence (PL). The SiV PL peak at 738 nm represents ZPL of SiV centers created in the NCD layers during growth. The presence of the peak at 738 nm is thus the proof of SiV centers existence in the NCD layer. In addition, the intensity of the PL peak is subject to changes in the NCD SiV layer composition and surface termination.[21–23] Hydrogenated surfaces decrease SiV PL intensity whereas oxidized surfaces give rise to a higher intensity.[21,23,24] By oxidizing the NCD surface, the electron affinity changes from negative to positive. SiV excited state near H-terminated diamond surface is thus above the Fermi level and photoexcited electrons recombine with hole in the surface conductive layer (SCL), effectively quenching SiV PL. The positive electron affinity of oxidized diamond surface means that the excited energy levels of the SiV centers in the surface layer are below the Fermi level, and photoexcited electrons can occupy these levels and contribute to PL emission of SiV centers.[23]

This kind of charging and recombination effects near surface can also be studied by electrical potential measurements. In particular, Kelvin probe force microscopy (KPFM) or scanning

Kelvin probe (SKP) methods have contributed to the study of physical phenomena on diamonds, such as surface potential, charge transfer, photovoltage (PV), and work function (WF).[25–30] The WF of the hydrogenated diamond surface was investigated by KPFM in many prior publications.[25,26] The SKP method significantly helped to understand photogenerated charge transfer from perylene diimide to boron-doped diamond.[27] Using PL and KPFM, Stehlik et al.[24] studied the optoelectronic properties of SiV centers in ultrathin (7–40 nm) NCD films with hydrogenated and oxidized surfaces. The study showed that the PV changes with the thickness of the layer, and the polarity was influenced by surface modification. Positive PV for O-terminated approached zero at 10 and 40 nm NCD film thickness. H-terminated NCD films showed negative PV increase with increased thickness. The WF decreased with increasing thickness and approached values typical for bulk diamonds. For O-terminated surface, the trend in PV was nonmonotonous. The KPFM and PV measurements were performed in glove box and all the samples were annealed at 250 °C for 1 h prior to the KPFM/PV measurement to exclude the effect of water adsorbed on the surface. The illumination was by a supercontinuum laser with 695 nm selected.

In the present work we focus on studying PVs arising from excitation of SiV centers under ambient condition and under broadband solar illumination to explore also possible energy harvesting effects through these quantum centers. We use the SKP setup with a steel tip in a closed box under ambient environment, where it is possible to achieve fully dark conditions, unlike in the KPFM system employing laser diode for sensing. In addition, the solar simulator with built-in AM1.5G filter and spectral range 350–1100 nm is used for the sample illumination.

We characterize NCD films with SiV centers as a function of thickness where the thickness of layers with SiV centers is controlled by the NCD growth time (3–60 min) and spans across much wider range from 10 to 200 nm. We modify surfaces of the grown layer in hydrogen or oxygen plasma. We compare the WF and surface photovoltaic voltage (SPV) as a function of thickness with different NCD surface modifications. We show that SPV polarity and amplitude change with the layer thickness in a pronounced way and in a similar way on both types of surfaces. We propose and discuss a model to explain the observed effects.

2. Experimental Section

2.1. Sample Preparation

Figure 1a shows the scheme of the SiV NCD thin film samples. Thin diamond films were grown on $10 \times 10 \, mm^2$ Si (100) substrates. Before the chemical vapor deposition (CVD) growth, substrates were cleaned and ultrasonically pretreated in a suspension of deionized water and dispersed detonation diamond powder (diameter 5–10 nm, New Metals and Chemicals Corp. Ltd., Kyobashi).[31] The CVD deposition of diamond was performed in a microwave (MW, 2.45 GHz) plasma-enhanced CVD reactor using the ellipsoidal resonator with focused plasma.[32] Diamond films were grown from hydrogen-rich plasma with methane (3% CH_4 in H_2, H_2 flow 300 sccm), total gas pressure 6 kPa and MW power of 3 kW, and temperature

about 700 °C. Additional pieces of bare clean Si substrates as well as the nucleated substrates themselves served as a source of Si atoms. Based on this deposition setup as well as prior reports in the literature (e.g., ref. [21]), we believe that the SiV concentration is not significantly dependent on the layer thickness. The thickness of the grown diamond layers was controlled by the CVD deposition time. A total of six thin SiV NCD layers were prepared with the growth times between 3 and 15 min, corresponding to the grown thickness range 10–50 nm (see **Table 1** for specific values) as well as two thicker reference samples of 90 and 200 nm thickness. The surfaces of as-grown NCD films were oxidized or hydrogen-terminated. For the surface oxidation, an ICP radio frequency (RF, 13.56 MHz) plasma system with the following parameters was used: RF power 100 W, pressure 60 Pa, O_2 flow rate 25 sccm, and process time 4 min. For the hydrogen-terminated surface, the same MW plasma-enhanced CVD system as used for the growth of the diamond films was used for 10 min without CH_4 addition at otherwise the same other conditions.

2.2. Methods

The film thickness of the prepared samples was determined by two methods. First method was scanning electron microscopy (SEM). The SEM images of NCD films were acquired at 10 kV and magnification of 200 kX (MAIA 3, Tescan, Czech Republic) in the regime of secondary electrons (SE) using an in-beam detector. Working distance (WD) was 4.66 mm. Each prepared sample was cut into two pieces, and the layer thickness was determined by measuring the cross section of the sample at three positions where the thickness was read at 10 points. The procedure was repeated for the samples with both surface modifications. Cross-sectional morphology images are shown in Figure 1b. The obtained thickness values were averaged and the standard deviation was calculated. Determining the thickness by SEM on NCD SiV was challenging due to the very thin layer and low contrast so we decided to verify the thicknesses of NCD SiV with the second method. The second method used for layer thickness determination was reflectance interferometry. This method uses spectroscopic reflectometer Ocean Optics NanoCalc-XR and NanoCalc software for data evaluation down to 5 nm thickness. A thin diamond layer was illuminated with the 90° incidence angle white light in the 250–1050 nm range. The corresponding optical model analyzed the reflected light as a wavelength function. The thickness data from the both methods are summarized in Table 1. Sometimes the SEM and reflectometry thickness is close, sometime not. As the reflectometry measures from the lager area, we assume the values to be more representative and they are used further on for plotting and analyzing the thickness dependencies.

Note that the DND nucleation layer is included in the total film thickness. The thickness of the nucleation phase was studied in one of our previous works[33] where the thickness of the nucleation layer ranged from 20 to 30 nm. Thus, we take 25 nm as the average nucleation layer thickness. The thickness of the actually grown NCD layer with SiV centers has been estimated by subtracting the average thickness of the DND nucleation layer. Yet, for the purpose of clarity only the total sample thickness will be used in graphs further on.
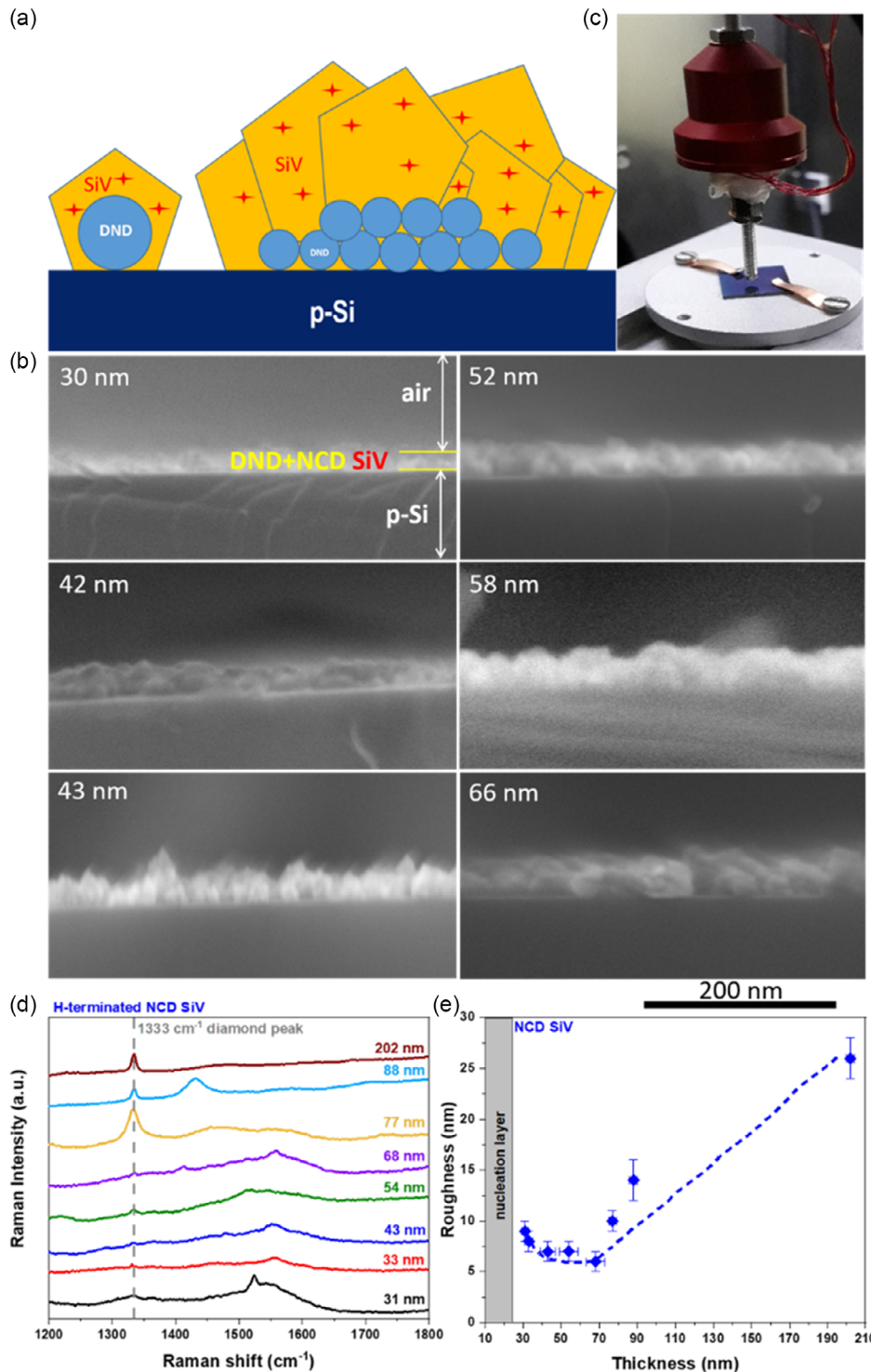
Figure 1. a) Scheme of NCD SiV samples. b) SEM cross-sectional morphology images (SE) with indicated average layer thicknesses. c) Photograph of the SKP probe head with an SiV NCD sample underneath contacted by clamps. d) H-terminated NCD SiV Raman spectra for individual layer thicknesses (due to a high Raman intensity on 88 and 202 nm, those spectra were divided by a factor of 10). e) Surface roughness (root mean square) related to various NCD SiV layer thicknesses (indicated trend line is guide for an eye).

The NCD SiV samples chemical composition was obtained using a confocal Raman microscope (WITec *alpha300* RAS) equipped with a green light laser (excitation wavelength 532 nm, laser power five mW). Raman spectra were collected in two different points by 100× objective (NA 0.9) and UHTS 300 VIS spectrometer. The integration time was 20 min for

VI

Table 1. Average thicknesses of the studied SiV NCD samples: total sample thickness based on SEM measurements and estimated thickness of the grown SiV NCD layer after subtraction of average nanodiamond nucleation layer thickness (25 nm).

Sample no.	1	2	3	4	5	6	7	8
Total film thickness determined by SEM [nm]	30 ± 2	42 ± 1	52 ± 5	58 ± 8	43 ± 1	66 ± 2	90 ± 5	200 ± 5
Total film thickness determined by spectroscopic reflectometer [nm]	31 ± 2	33 ± 2	43 ± 4	54 ± 5	68 ± 5	77 ± 2	88 ± 2	202 ± 2
Grown SiV NCD layer thickness [nm]	6 ± 2	8 ± 1	18 ± 1	29 ± 5	43 ± 8	52 ± 2	63 ± 5	177 ± 5

samples with thinner NCD SiV layers and 5 min for reference samples with layer thicknesses of 90 and 200 nm. Spectra were collected and processed by WITec Control 6.1 and WITec Project 6.1 software. Raman spectra for H-terminated NCD SiV samples are shown in Figure 1d and for O-terminated in Figure S1, Supporting Information. The Raman intensity was divided by a factor of 10 for NCD SiV with layer thicknesses of 88 and 202 nm to better compare them with NCD SiV spectra of lower thickness. Raman spectra confirm the presence of a diamond peak at 1333 cm^{-1} in all NCD SiV samples albeit with different intensity depending on layer thickness. In addition to the diamond peak in the spectra, the carbon D-band at 1451 cm^{-1} and graphitic band of sp^2 at 1591 cm^{-1} are detected in all samples.[34,35]

The atomic force microscopy (AFM—LiteScope 2.0, NenoVision) obtained morphology information in semicontact mode, frequency shift, and amplitude of cantilever oscillations using an Akiyama self-sensing and self-actuating probe based on the tuning fork method. An electrical signal was sent to the probe to make it resonate, and the change in this resonance frequency corresponds to changes in the surface. The obtained AFM data were processed by software Gwyddion 2.62.[36] Figure 1e shows the dependence of the roughness on the thickness of the H-modified SiV NCDs. Roughness for O-terminated NCD SiV was not shown as we assume that the roughness values for O-terminated NCD SiV are within the error for H-terminated NCD SiV. Roughness values are higher for thin NCD SiV films (31 and 33 nm) due to shorter growth time and more significant pores/gaps between NCDs. As the layer thickness increases, the gaps are filled, and at film thicknesses of 43 and 54 nm, the roughness is lower and changes minimally. The roughness for NCD films with a thickness higher than 68 nm increases again due to the growth of NCD crystallites. Overview of all topographies is shown in Figure S2, Supporting Information. Note that the tip used to measure the topography was slightly blunt and there is a slight offset in the topography, yet generally the morphology is following the trend in surface roughness.

The morphology of NCD SiV with different layer thicknesses was also obtained by SEM (Zeiss EVO 10). The SEM images of NCD films were acquired at 10 kV and magnification of 20 kX in the regime of SE using an off-beam detector. WD was 8.18 mm. The representative SEM morphology images for each sample are shown in Figure S3, Supporting Information. The electronic structure appears generally homogeneous across all the sample surfaces. Darker contrast for samples with lower NCD SiV thickness and brighter for NCD SiV with higher thickness is generally observed, indicating the effect of subsurface electronic properties on the SE emission. Surprisingly, NCD SiV with a layer thickness

of 88 nm had a darker brightness than expected and showed results slightly off the main trend also in almost all other experiments.

The PL spectra were measured using confocal PL microscope (WITec *alpha300* RAS) equipped with white light continuum source (SuperK Extreme, NKT Photonics) and spectral filtering module (SuperK Varia, NKT Photonics), 100× objective (NA 0.9), and UHTS 300 VIS spectrometer. A 700 nm short pass and 700 nm long pass spectral filters were placed into the excitation and the PL collection path, respectively, in order to prevent the laser light from leaking into spectrometer. Two excitation wavelengths (550 and 650 nm) were used with 10 nm bandwidth in each case, and average intensity 1.42 and 1.1 mW incident on the sample, respectively. PL spectra were measured on multiple spots on the sample and a mean value and its uncertainty was computed. Representative spectra for each sample are shown in Figure S4, Supporting Information. For analysis, the measured spectra were fitted by a function defined as a sum of broad Gaussian function (broad PL band originating from defects in NCD), narrow pseudo-Voigt function (SiV center ZPL), and Gaussian function (SiV phonon sideband). Pseudo-Voigt function fits the ZPL better than Lorentzian or Gaussian function alone, which is most probably caused by nonhomogeneous broadening of the line due to variable environment (stress, presence of other defects) that acts on individual SiV centers within the detected volume. The SiV ZPL intensity was determined as an area of the pseudo-Voigt function fitted to the measured spectra.

Contact potential difference (CPD) was measured by the scanning Kelvin probe method (KP Technology, UK). Figure 1c shows photograph of the SKP probe head with an SiV NCD sample underneath that is contacted by clamps. The CPD data were recalculated to the WF values using the following equation:

$$\mathrm{WF_{sample}} = (\mathrm{CPD_{sample}} - \mathrm{CPD_{ref}}) \times 10^{-3} + \mathrm{WF_{ref}} \qquad (1)$$

As the WF reference (WF$_{ref}$), an Au reference sample from KP Technology was used. SKP measurements were done in a glove box using a grounded steel probe tip of 2 mm diameter. The sample charge was stabilized by 7 min illumination before CPD was measured. The CPD was measured in the light–dark–light cycle switched on/off the light (simulated sunlight using AM1.5G filter, class AAA solar simulator HAL-C100, Asahi Spectra, Japan), equipped with AM 1.5G filter. In the dark, the WF values reflect the intrinsic material properties and possibly retained electrostatic charge. Under illumination, the difference in WF corresponds to PV generation on the sample surface. Lower WF (CPD) values correspond in our setup to positive PV, i.e., to

VII

the generation/transfer of holes on the surface. The CPD was measured as a function of time for 7 min (750 data points). Multiple locations were tested on each sample.

3. Results and Discussion

3.1. Kelvin Probe Measurements

The WF and surface PV were measured by Kelvin probe in the dark and under illumination in the cycle of light–dark–light. **Figure 2** shows graphs with typical results of CPD measurements on H-terminated (Figure 2a) and O-terminated (Figure 2b) SiV NCD with different layer thicknesses. The yellow area represents surface potential measured under illumination and the gray area represents surface potential measured in the dark. Potential profiles in the graphs include information about the NCD WF,
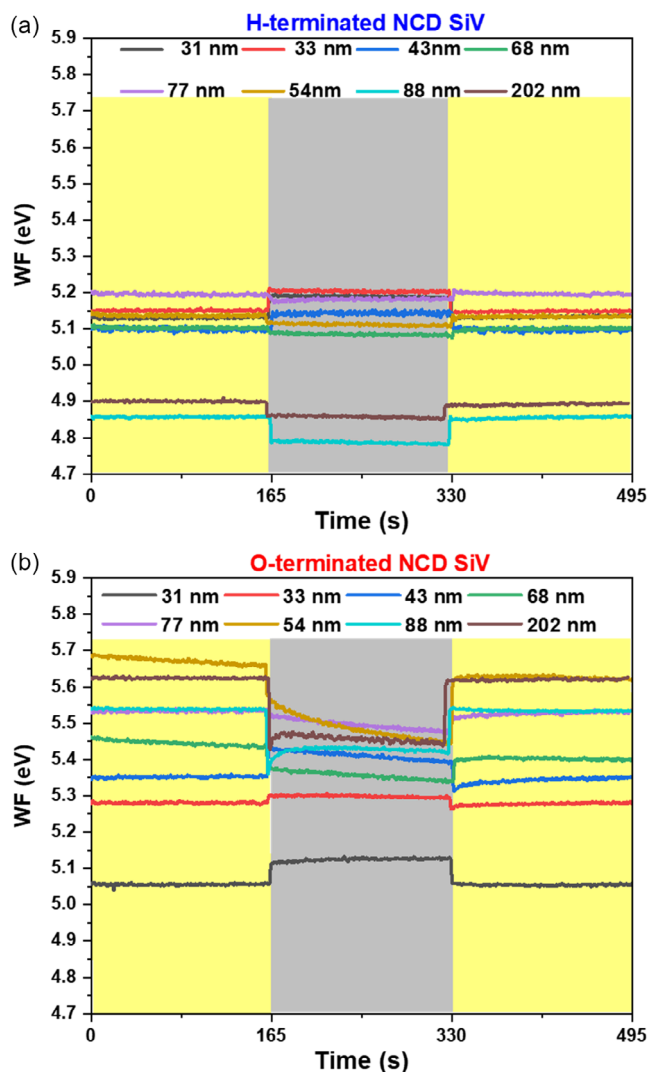
kinetic behavior of surface potential, and photogenerated charges.

For H-terminated NCDs, the surface potential is stable under illumination and slightly drifting in the dark, in particular for higher NCD thicknesses. It seems that the NCD samples are discharging in the dark. The significant drifting observed in the dark measurements was the reason for the illumination (light soaking) of the samples 7 min before the SKP measurements by a solar simulator. It reduced the overall drift. It looks like the illumination stabilizes the NCD surface charges.

From the potential profiles one can see that the actual sample WF in dark and PV generated under illumination are not uniform. The value as well as direction of response strongly varies with the sample thickness. **Figure 3** shows analysis of the WF and SPV values from multiple measurements plotted as a function of the total film thickness. Average thickness of the nucleation layer is indicated by the gray rectangle. The white part of the graph thus corresponds to the grown NCD layer with SiV centers.
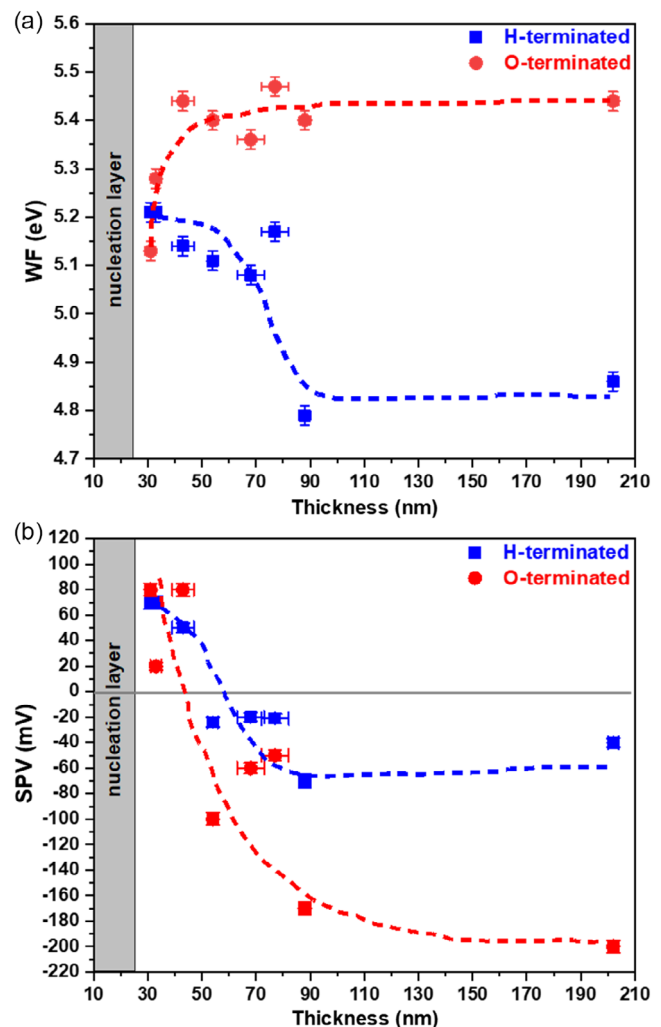

Figure 2. Time-resolved Kelvin probe measurements in the dark (gray area) and under illumination by solar simulator (yellow area) for different layer thickness and surface modifications: a) hydrogenated NCD SiV; b) oxidized NCD SiV.

Figure 3. a) WF and b) surface PV for H-terminated and oxidized NCD films with SiV centers. Approximate thickness of the nucleation layer made of detonation nanodiamonds (without SiV centers) is indicated by the gray area. Indicated trend lines serve as guides for an eye.

VIII

Figure 3a shows the WF in the dark for the studied NCD SiV samples with hydrogenated (blue) and oxidized (red) surfaces. The WF for the H-terminated SiV NCD generally decreases with the layer thickness. The highest WF value of 5.2 eV is for the sample with the lowest thickness. There is also a noticeable plateau at the lowest thicknesses where the WF of H-terminated NCD changes only weakly (within 0.1 eV), most likely related with SCL effects as such plateau is not observed on oxidized layers of the same thickness. Then the WF decreases and saturates for higher thicknesses at around 4.8–4.9 eV, in agreement with expectations for H-terminated bulk diamond surfaces.[30] On the other hand, the WF for O-terminated NCD directly increases with thickness from 5.1 to 5.5 eV at 68 nm and then it also becomes saturated at about the same level which is in agreement with the expected values for bulk diamond.[37] Obviously, the most pronounced variations of NCD WF occur below 88 nm film thickness (i.e., below 63 nm of actually grown SiV NCD layer thickness) for both H-terminated and oxidized surfaces. Similar values of WF for both H-terminated and oxidized surfaces at small NCD layer thicknesses can be explained by charging as observed on the nanodiamond clusters and thin films.[38] In addition, we compared the NCD values of SiV WF with surface roughness (see the roughness values plotted in Figure 1e). Roughness trend is not monotonous (in agreement with reports in the literature on NCD growth) and obviously does not correlate with the WF or SPV trends. Both WF and SPV follow the increase in thickness monotonously. Moreover, WF values decrease with increased thickness on H-terminated samples whereas WF values increase with increased thickness on O-terminated samples. At the most pronounced roughness increase (from 88 to 202 nm samples), the WF and SPV almost do not change.

Figure 3b shows SPV evaluated for NCD SiV samples with an H-terminated surface (blue color) and an O-terminated surface (red color). The NCD samples with a layer thickness of 30–43 nm (thin NCD layer < 50 nm) generated positive PV both for H-terminated and O-terminated surfaces. On the other hand, samples with a thicker layer (50 nm), generated a negative SPV. The SPV switched polarity at a layer thickness of 50 nm. The thickness of 50 nm (effectively 25 nm SiV NCD layer, without DND nucleation layer) thus represents a halfway boundary between surface-controllable and bulk SiV centers dominant contribution. NCDs with layer thickness higher than 50 nm generated negative SPV as bulk diamonds[26,28] or boron-doped diamonds.[27] Also SPV in the ultrathin SiV NCD films start to approach zero around 40 nm[24] although the switch of polarity was not observed and the experiment was performed under different conditions and the data is not directly comparable.

Figure 4a shows PL intensity dependence on H-terminated (blue points) and O-terminated (red points) NCD SiV layer thickness at excitation wavelength 550 nm. SiV centers did not show PL excitation on the thinnest NCD SiV layers (31 nm) for both surface modifications. The low PL intensity was observed for NCD SiV film thickness of 33 nm, and PL intensity increased exponentially with increasing NCD SiV thickness for O-terminated samples. On the other hand, H-terminated NCD SiV showed very low luminescence at layer thickness 43 nm and did not significantly change up to thickness 68 nm when the PL signal started to rise significantly. Figure 4b also
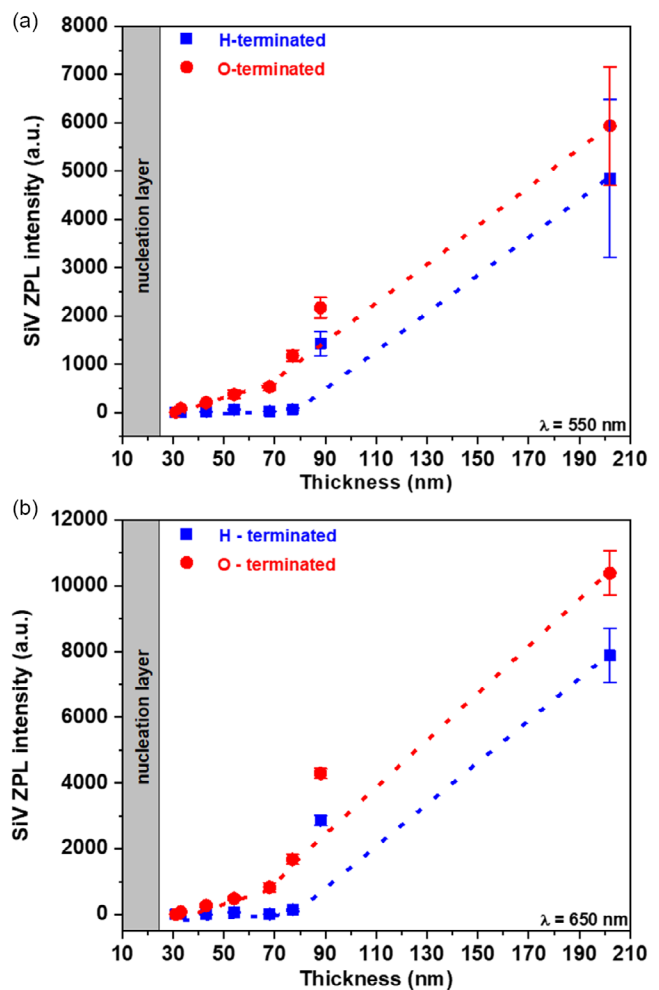

Figure 4. Dependence of the NCD SiV centers on layer thickness for H-terminated and O-terminated surfaces, measured with excitation wavelength a) 550 nm and b) 650 nm. Indicated trend lines serve as guides for an eye.

shows the dependence of the PL intensity change on the layer thickness for excitation wavelength 650 nm. Again we observed similar trends where SiV centers provided luminescence at NCD SiV layer thickness 33 nm for O-terminated surface and 54 nm for H-terminated samples. Both excitation wavelengths show a high increase in PL intensity ratio for an NCD SiV layer thickness of 88 nm for both surface modifications, H-terminated and O-terminated, probably caused by the sample material difference already indicate by the SEM images. Furthermore, both excitation wavelengths showed luminescence switching points at NCD SiV layer thickness of 33 nm for O-terminated and 54 nm for H-terminated. SiV PL intensity data correlate well with the WF and SPV data. It is obvious that PV switches from positive to negative with the onset of SiV PL intensity rise. Zero or very low PL corresponds to positive PV and no or small changes in the WF (see Figure 3). Further increase in luminescence correlates with the rise in the WF on O-terminated NCD SiV or the decrease in WF on H-terminated NCD SiV, both approaching bulk WF values. Of course, it is not only the WF value that controls

the SiV PL intensity, a subsurface energetic band profiles must be considered.

The above observations can be explained by the following mechanisms that are schematically illustrated in **Figure 5**. On H-terminated SiV NCD films, we assume, due to the ambient environment, the presence of the p-type SCL with Fermi-level energy below the valence band maximum.[26,30] This brings the excited energy level as well as ground state (that is at or below valence band maximum) of SiV centers above the Fermi level in the surface vicinity. The PL of SiV is quenched in this situation. It could be due to change of near-surface SiV^- to SiV^0 but no corresponding PL at 946 nm was observed.[24] It is thus more likely that while electrons at or below Fermi level are excited by illumination to the SiV center, the electrons will tend to get to SiV of lower energies toward the sample depth whereas related holes will become delocalized in the SCL and be drawn toward the surface and even trapped in surface states (existing due to imperfections of NCD also on H-terminated surfaces but in much lower density than on oxidized surfaces) or sp^2 carbon phase,[39] thereby increasing surface positive charge and inhibiting the SiV PL. As the thickness of the layer increases, the photoexcited SiV centers will contribute with increasing positive charge (holes) toward the surface, until the excited SiV level will get below the Fermi level. This depth corresponds to about a double of SCL depth (which has been estimated to 7–13 nm). A slight increase or at least a plateau in the SPV is indeed noticeable in Figure 3b. When in the thicker layers the SiV centers are below the Fermi energy deeper in the layer, they contribute to SPV in opposite way, thereby compensating the originally net positive charge to zero. It will be approximately at the depth corresponding to quadruple of SCL depth, i.e., between 20 and 40 nm of the grown SiV layer thickness. The SPV in Figure 3b indeed goes through zero in this area (45–65 nm when we account for the nucleation layer thickness). The negative charge increases until the SiV centers are too deep in the layer to contribute to surface charge and SPV is saturated at the value of about −50 mV.

Figure 5b illustrates the SPV mechanism in oxidized SiV NCD layer. The bands are bent upward but the Fermi level is pinned due to a high density of surface states (around 1.8–2.2 eV above the valence band) that act as hole traps.[40] Thus, the SiV system remains fully below the Fermi level and SiV PL is higher than on similarly thin H-terminated samples. For the thin NCD layers, the photoexcited holes on the SiV centers become trapped on the surface states.[24] The hole trapping is further promoted by the upward surface band banding that helps holes move toward the surface. This effect leads to dominant positive surface charge when the NCD layer thickness is within the band bending range. As the thickness increases, the deeper SiV centers start again to contribute with negative charge to SPV (as in the case of H-terminated samples). This leads to decrease and full compensation of the positive SPV, approximately at double band bending depth. Net negative SPV then starts to prevail and becomes saturated at the value of about −200 mV. For the larger thicknesses, the SiV centers are too deep in the layer to contribute.

The proposed mechanism may appear too simplified, not considering grain boundaries, nondiamond carbon phases, silicon–diamond bottom junction, and various other factors. Yet already at this level it seems fully consistent with the presented data. The detailed mechanism of how the electrons from photoexcited SiV get to the surface still remains to be elucidated though. For more detailed insight, experiments with tunable laser illumination (400–800 nm) are ongoing.
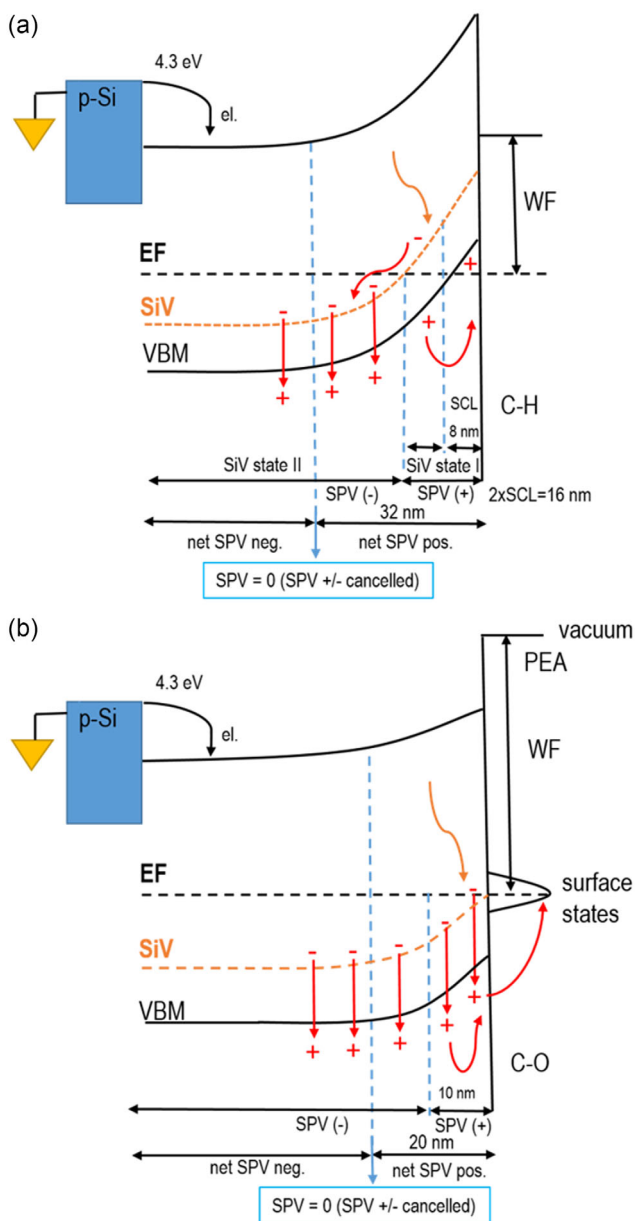

Figure 5. Proposed thickness dependent band diagram model of PV generation and polarity switching for a) H-terminated and b) O-terminated SiV NCD layers.

4. Conclusions

SiV NCD samples with different film thicknesses (30–200 nm) and H-terminated and O-terminated surfaces were studied by the scanning Kelvin probe method in the dark and under solar simulator illumination. The WF in the dark and SPV generated

under illumination are not uniform. The value as well as the direction of the response varied with the thickness of the sample. The change in WF for H-terminated samples at low thicknesses is weak, while for O-terminated samples WF increases by 0.4 eV. At high thicknesses, WF showed values typical for bulk diamonds for both types of surfaces. SPV amplitude and polarity changed with the SiV NCD layer thickness. Positive SPV was observed for film thickness below 55 nm. SiV NCD films with thicknesses above 55 nm generated negative SPV. Diamond samples with a layer thickness of about 55 nm represent the halfway boundary between surface-controllable SiV centers and SiV in diamond bulk. The photovoltaic voltage switching mechanism was explained using a band diagram considering effects in the surface band bending region. The value of 55 nm corresponds to about 30 nm of the actually grown SiV NCD layes, which is about 4 times the surface band bending due to surface conductive layer on H-terminated surface or surface states on oxidized surface. The study may contribute to employing SiV color centers for energy harvesting applications as well as for general understanding and control of the SiV centers for other diverse applications.

Supporting Information

Supporting Information is available from the Wiley Online Library or from the author.

Acknowledgements

Conflict of Interest

The authors declare no conflict of interest.

Data Availability Statement

The data that support the findings of this study are available from the corresponding author upon reasonable request.

Keywords

[1] L. Tang, C. Tsai, W. W. Gerberich, L. Kruckeberg, D. R. Kania, *Biomaterials* **1995**, *16*, 483.

[2] S. N. Wuersching, C. Högg, L. Kohl, F.-X. Reichl, R. Hickel, M. Kollmuss, *Dent. Mater.* **2023**, *39*, 293.

[3] C. E. Nebel, *Nat. Mater.* **2003**, *2*, 431.

[4] D. Shin, B. Rezek, N. Tokuda, D. Takeuchi, H. Watanabe, T. Nakamura, T. Yamamoto, C. E. Nebel, *Phys. Status Solidi A* **2006**, *203*, 3245.

[5] M. A. Lodes, F. S. Kachold, S. M. Rosiwal, *Phil. Trans. R. Soc. A* **2015**, *373*, 20140136.

[6] P. Hollman, O. Wänstrand, S. Hogmark, *Diamond Relat. Mater.* **1998**, *7*, 1471.

[7] S. J. Askari, G. C. Chen, F. Akhtar, F. X. Lu, *Diamond Relat. Mater.* **2008**, *17*, 294.

[8] S. Kumar, M. Nehra, D. Kedia, N. Dilbaghi, K. Tankeshwar, K.-H. Kim, *Carbon* **2019**, *143*, 678.

[9] M. Krátká, O. Babchenko, E. Ukraintsev, J. Vachelová, M. Davídková, M. Vandrovcová, A. Kromka, B. Rezek, *Diamond Relat. Mater.* **2016**, *63*, 186.

[10] A. Härtl, E. Schmich, J. A. Garrido, J. Hernando, S. C. R. Catharino, S. Walter, P. Feulner, A. Kromka, D. Steinmüller, M. Stutzmann, *Nat. Mater.* **2004**, *3*, 736.

[11] P. Niedziałkowski, Z. Cebula, N. Malinowska, W. Białobrzeska, M. Sobaszek, M. Ficek, R. Bogdanowicz, J. S. Anand, T. Ossowski, *Biosens. Bioelectron.* **2019**, *126*, 308.

[12] I. Harris, C. J. Ciccarino, J. Flick, D. R. Englund, P. Narang, *Phys. Rev. B* **2020**, *102*, 195206.

[13] N. Felgen, A. Schmidt, B. Naydenov, F. Jelezko, J. P. Reithmaier, C. Popov, *NATO Sci. Peace Secur. Ser. B* **2018**, 193.

[14] T. Müller, C. Hepp, B. Pingault, E. Neu, S. Gsell, M. Schreck, H. Sternschulte, D. Steinmüller-Nethl, C. Becher, M. Atatüre, *Nat. Commun.* **2014**, *5*, 3328.

[15] K. D. Jahnke, A. Sipahigil, J. M. Binder, M. W. Doherty, M. Metsch, L. J. Rogers, N. B. Manson, M. D. Lukin, F. Jelezko, *New J. Phys.* **2015**, *17*, 043011.

[16] J. N. Becker, C. Becher, *Phys. Status Solidi A* **2017**, *214*, 1700586.

[17] J. Riedrich-Möller, C. Arend, C. Pauly, F. Mücklich, M. Fischer, S. Gsell, M. Schreck, C. Becher, *Nano Lett.* **2014**, *14*, 5281.

[18] K. G. Fehler, A. P. Ovvyan, L. Antoniuk, N. Lettner, N. Gruhler, V. A. Davydov, V. N. Agafonov, W. H. P. Pernice, A. Kubanek, *Nanophotonics* **2020**, *9*, 3655.

[19] E. Neu, M. Agio, C. Becher, *Opt. Express* **2012**, *20*, 19956.

[20] E. Neu, D. Steinmetz, J. Riedrich-Möller, S. Gsell, M. Fischer, M. Schreck, C. Becher, *New J. Phys.* **2011**, *13*, 025012.

[21] S. Stehlik, M. Varga, P. Stenclova, L. Ondic, M. Ledinsky, J. Pangrac, O. Vanek, J. Lipov, A. Kromka, B. Rezek, *ACS Appl. Mater. Interfaces* **2017**, *9*, 38842.

[22] Š. Potocký, T. Ižák, M. Varga, A. Kromka, *Phys. Status Solidi B* **2015**, *252*, 2580.

[23] B. Yang, B. Yu, H. Li, N. Huang, L. Liu, X. Jiang, *Carbon* **2020**, *156*, 242.

[24] S. Stehlik, L. Ondic, M. Varga, J. Fait, A. Artemenko, T. Glatzel, A. Kromka, B. Rezek, *Micromachines* **2018**, *9*, 281.

[25] J. H. Lay, K. M. O'Donnell, P. W. May, *Chem. Phys. Lett.* **2011**, *515*, 151.

[26] B. Rezek, C. E. Nebel, M. Stutzmann, *Diamond Relat. Mater.* **2004**, *13*, 740.

[27] D. López-Carballeira, J. Raymakers, A. Artemenko, R. Lenaerts, J. Čermák, J. Kuliček, S. S. Nicley, A. Kromka, K. Haenen, W. Maes, B. Rezek, *Sol. Energy Mater. Sol. Cells* **2022**, *248*, 111984.

[28] Th Dittrich, *AIP Adv.* **2022**, *12*, 065206.

[29] D. Miliaieva, P. Matunova, J. Cermak, S. Stehlik, A. Cernescu, Z. Remes, P. Stenclova, M. Muller, B. Rezek, *Sci. Rep.* **2021**, *11*, 590.

[30] B. Rezek, C. Sauerer, C. E. Nebel, M. Stutzmann, J. Ristein, L. Ley, E. Snidero, P. Bergonzo, *Appl. Phys. Lett.* **2003**, *82*, 2266.

[31] A. Kromka, Š. Potocký, J. Čermák, B. Rezek, J. Potměšil, J. Zemek, M. Vaněček, *Diamond Relat. Mater.* **2008**, *17*, 1252.

[32] M. Füner, C. Wild, P. Koidl, *Appl. Phys. Lett.* **1998**, *72*, 1149.

[33] A. Kromka, B. Rezek, Z. Remes, M. Michalka, M. Ledinsky, J. Zemek, J. Potmesil, M. Vanecek, *Chem. Vap. Deposition* **2008**, *14*, 181.

[34] R. Haubner, M. Rudigier, *Phys. Procedia* **2013**, *46*, 71.

[35] O. Babchenko, T. Izak, E. Ukraintsev, K. Hruska, B. Rezek, A. Kromka, *Phys. Status Solidi B* **2010**, *247*, 3026.

[36] D. Nečas, P. Klapetek, *Open Phys.* **2012**, *10*, 181.

[37] F. Maier, J. Ristein, L. Ley, *Phys. Rev. B* **2001**, *64*, 165411.

[38] S. Stehlik, T. Petit, H. A. Girard, J.-C. Arnault, A. Kromka, B. Rezek, *Langmuir* **2013**, *29*, 1634.

[39] E. Verveniotis, A. Kromka, M. Ledinský, B. Rezek, *Diamond Relat. Mater.* **2012**, *24*, 39.

[40] Y. Itoh, Y. Sumikawa, H. Umezawa, H. Kawarada, *Appl. Phys. Lett.* **2006**, *89*, 203503.